Carrier Lifetimes and Electric Fields of Geometrically Asymmetrical MoS_2 Devices

by

Levi Holmes

Thesis Submitted in Partial Fulfillment of the
Requirements for the Degree of
Engineering Physics Undergraduate

in the
Department of Engineering

SIMON FRASER UNIVERSITY
Fall 2023

APPROVAL

Name: Levi Holmes

Degree: Bachelor of Applied Science Honours

Title of Thesis: Charge Transport Characterization & Lifetime of Geometrically Asymmetrical MoS2 Devices

Dr. Cheng Li, P.Eng.
Director, School of Engineering Science

Examining Committee:

Dr. Michael Adachi, P.Eng.
Professor, School of Engineering Science

Dr. Michael Hegedus
Professor, School of Engineering Science

Dr. Shawn Sederberg, P.Eng.
Professor, School of Engineering Science

Dr. Ash Parameswaran P.Eng.
Professor, School of Engineering Science

Date Approved: Dec. 19th, 2023

Declaration of Committee

Name:	**Levi Holmes**
Degree:	**Engineering Physics Undergraduate**
Thesis title:	**Carrier Lifetimes and Electric Fields of Geometrically Asymmetrical MoS_2 Devices**
Committee:	**Chair:** Michael Adachi Supervisor Assistant Professor, Engineering
	Ash Parameswaran Committee Member Professor, Engineering
	Mike Hegedus Committee Member Lecturer, Engineering
	Shawn Sederberg Committee Member Assistant Professor, Engineering

Abstract

This thesis details the electrical characterization of a new asymmetrical geometry molybdenum disulfide (MoS_2) photodiode using transient photovoltage (TPV) and transient photocurrent (TPC) techniques for the first time. The charge carrier lifetimes, charge densities, and built-in electric fields were determined and compared with literature. Charge carrier lifetimes in a primary device were found to be in the microsecond range which is two to three orders of magnitude higher than other reported carrier lifetimes. The carrier lifetimes showed a decrease with increasing charge density, which was determined to range between 10^{12} and 10^{15} cm^{-3}. The electric fields of two devices have been estimated throughout the length of each device and had a maximum strength of $1.5 \times 10^5 \frac{V}{m}$.

Keywords: Simon Fraser University; 2D nanostructures; MoS_2, Asymmetric contact geometry, Transient analysis

Acknowledgements

I would like to express my gratitude to Dr. Michael Adachi for his generous and continued support throughout this project. I would like to sincerely thank Amin Abnavi, Mohammad Reza Mohammadzadeh, and Ribwar Ahmadi for their insights, encouragement, and kindness. I would like to thank my family for their patience, understanding, and editing. I could not have done it without them.

Table of Contents

List of Figures

Chapter 1

Introduction

1.1 Transition Metal Dichalcogenides and 2D Materials

Transition metal dichalcogenide (TMD) nano structures are at the forefront of innovation in photovoltaic cells, continuously being created and studied in an effort to shape the future of solar energy systems. A parameter of photovoltaic cells that engineers are striving to continuously optimize is the cell efficiency. One important aspect of this efficiency is the charge carrier (electron or hole) lifetimes. Charge carrier lifetimes are important for solar harvesting devices because the longer the charge carrier lifetime, the higher the chance that the carrier will be collected and become current. Carrier lifetimes and how to optimize them are largely still a mystery in TMDs and this gives engineers and researchers motivation to understand carrier lifetimes in these materials so they can make new innovations towards TMD solar cell efficiency.

TMDs are capable of achieving atomic scale thicknesses, known as two dimensional (2D) materials, and are notable for their capacity to be engineered to achieve a single layer thickness, called a monolayer. Interest in TMDs began after the discovery of the first 2D nano material, Graphene, in 2004. This groundbreaking material proved to have great electronic potential as a superconductor, spurring a decade of intense research into TMDs to explore their electrical properties and potential applications [7]. Figure 1.1 summarizes the family of 2D materials and there photosensitive range, this photosensitive range strongly influences the possible applications of the material.

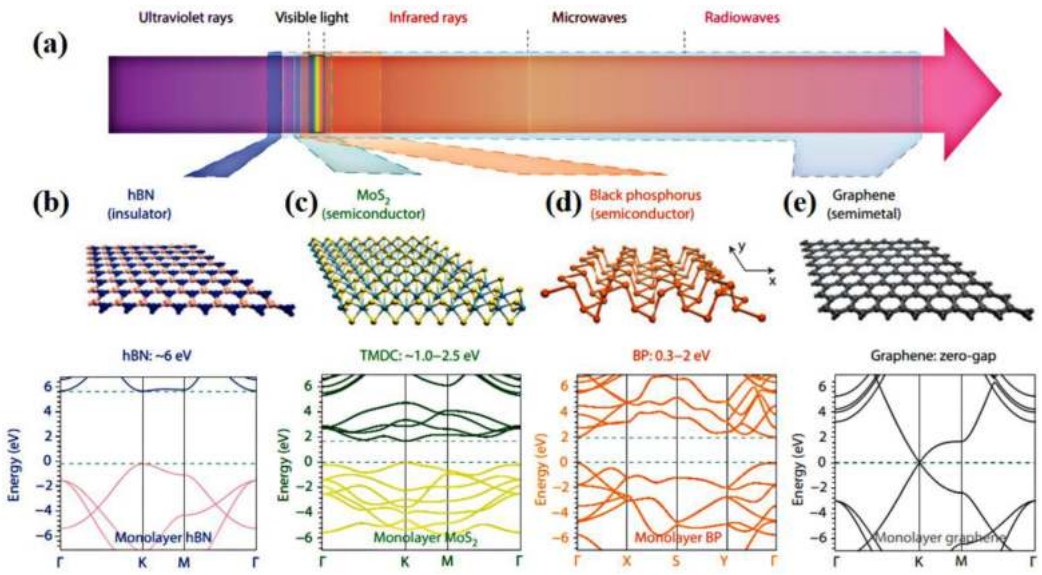

Figure 1.1: Examples of different types of 2D materials and their photosensitive range [1]

The attention to monolayer and multilayer nano structure TMDs is primarily due to the interesting electrical properties that TMDs exhibit at atomic scale thicknesses. These electrical properties manifest in various ways and with varying intensity as the material transitions from a bulk material to a monolayer. For example, transitioning to a monolayer shifts the bandgap energy from an indirect to a direct bandgap allowing the material to become photoluminescent. The bandgap energy, the most important property of a material in microelectronics, is what distinguishes a semiconductor from an insulator or a metal. This shift in the bandgap energy is depicted in Figure 1.2. Furthermore, this shifting phenomenon enables the bandgap to be engineered within a range of energies determined by the material, known as bandgap engineering [8]. This is possible because the bandgap energy is a function of the structural thickness of the device. The capacity to isolate TMD monolayers is rooted in their van der Waals bonds. These bonds have robust covalent bonds within the planes of the material, while simultaneously allowing van der Waals forces, essentially electrical dipoles, to govern the interactions between these planes. This structural aspect is pivotal in creating nano structures because this bond structure enables us to use mechanical exfoliation, a process by which layers can be peeled away from the bulk as depicted in Figure 1.3.

The change in electrical properties that occur in TMDs become maximized at the monolayer, where quantum effects become more apparent. For instance, an absence of an inversion center develops and allows for the spin of electrons to be controlled by tuning the excitation laser photon energy, thus adding a new degree of freedom to the charge carrier. Controlling the spin provides an opportunity to encode information in the spin of the electrons comprising the current. Spintronic systems are currently being realized in dilute magnetic

semiconductors (DMS), and are of particular interest in the field of quantum computing and neuromorphic computing [9].

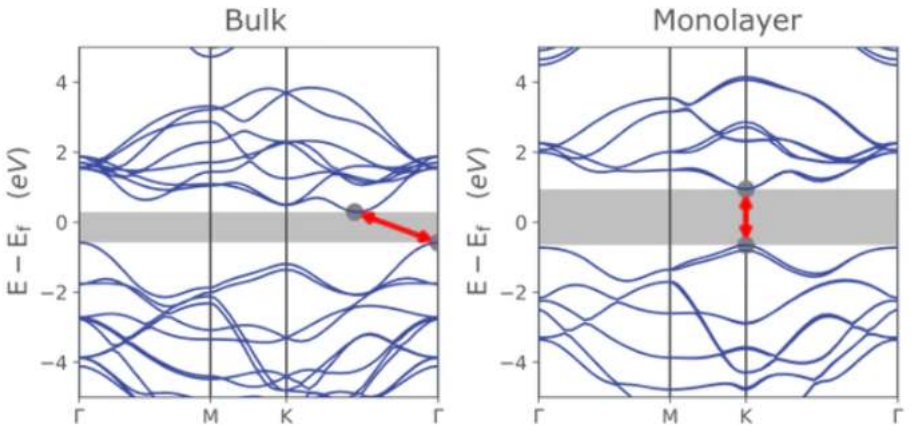

Figure 1.2: Band gap energy shifting from bulk to monolayer in MoS_2 [2]

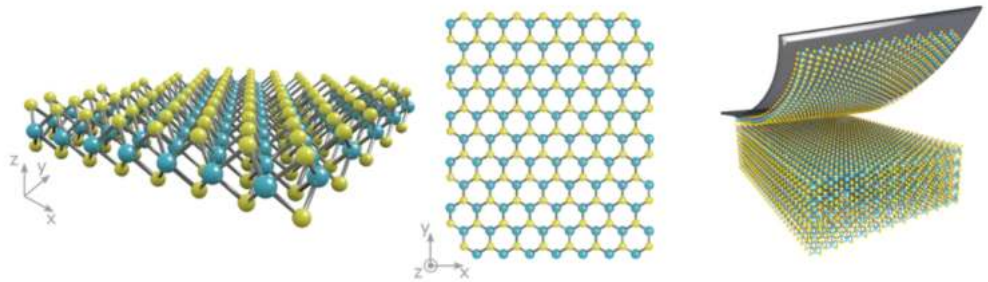

Figure 1.3: Monolayer structure of MoS_2 and the exfoliation method to fabricate monolayers [2]

1.2 MoS_2

Within the family of TMDs, MoS_2 stands out as one of the most extensively researched since 2010, when the first monolayer was successfully isolated by researchers revealing photoluminescent properties [10]. MoS_2 is particularly advantageous because of ease of fabrication and is less expensive to synthesize than other TMDs. MoS_2 has also been shown to have high photoresponsivity and absorption efficiency making it a promising material for photodetectors and solar cells [11]. Beyond performance and cost, MoS_2 has applications in areas ranging from gas sensing, photovoltaics, energy storage, wearable electronics, and even water decontamination [11]. Lastly, monolayer MoS_2 nanosheets are seen as one of the most appropriate supplementing materials to graphene for the fabrication of low power electronic devices [12].

MoS_2 has some drawbacks that are currently preventing it from being applied to mainstream electronics. One is its slow photoresponse dynamics, referring to its slower charge carrier mobility. This is where asymmetrical devices could be a step toward resolving that drawback [13].

1.3 Asymmetrical MoS_2

The new asymmetric contact geometry device was developed and investigated by the SFU Nano Device Fabrication Group (NDFG) in early 2022, where an analysis revealed that the device had the highest power conversion efficiency for a lateral 2D solar cell [3].

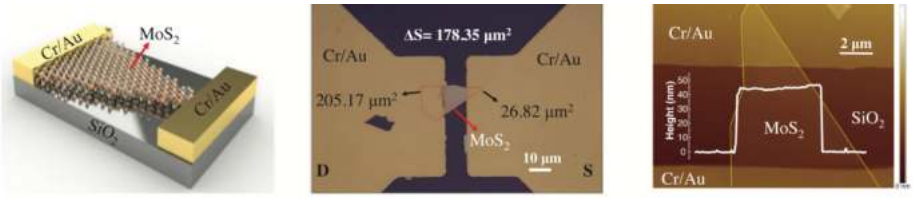

Figure 1.4: Asymmetrical geometry devices and profile fabricated by NDFG [3]

This simple innovation of asymmetrical contact geometry introduces a built-in electric field in between the contacts of the device. This allows it to be operated without any applied bias voltage, unlike symmetrical MoS_2 devices. The built-in electric field is a consequence of a Schottky barrier height mismatch. This height mismatch influences the direction of current, allowing the device to behave similarly to a silicon photodiode. The larger Schottky barrier corresponds to the smaller contact area and vice versa. The introduction of light on the device generates electrons with enough energy to cross the lower Schottky barrier. An electric current is produced as a result of these electrons being directed by the built-in electric field. The physical interpretation of why the carriers drift to one contact is still under investigation. A diagram of these unequal barrier heights from Abnavi et al (2022). can be viewed in Figure 1.5 below.

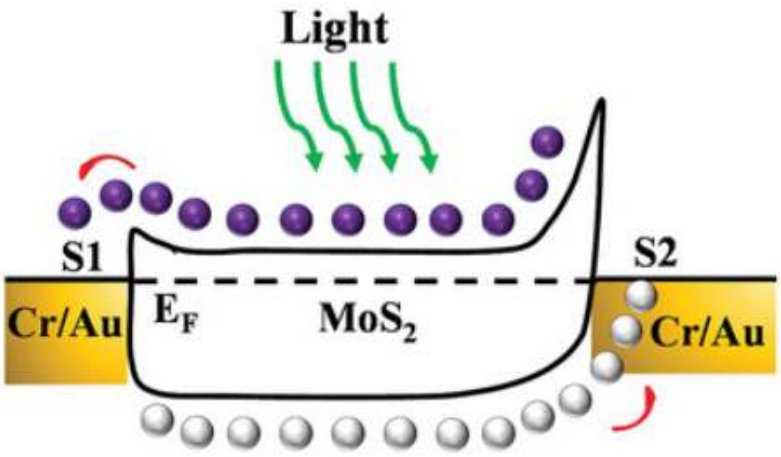

Figure 1.5: Unequal Schottky barrier heights resulting from uneven Schottky contact areas [4]

The asymmetrical geometry results in an asymmetrical photovoltage amplitude output, allowing the position of an incident photon flux from a laser to be determined from the output voltage signal. The signal strength and polarity of the photovoltage are dependent on location of the incident photons. This behavior is believed to originate from a combination of the contact asymmetry and the lateral charge collection [6]. As a result, this material shows potential for applications in position-sensitive detectors, which are crucial in particle detection and robotics. A depiction of an asymmetric voltage response can be found in Figure 1.6.

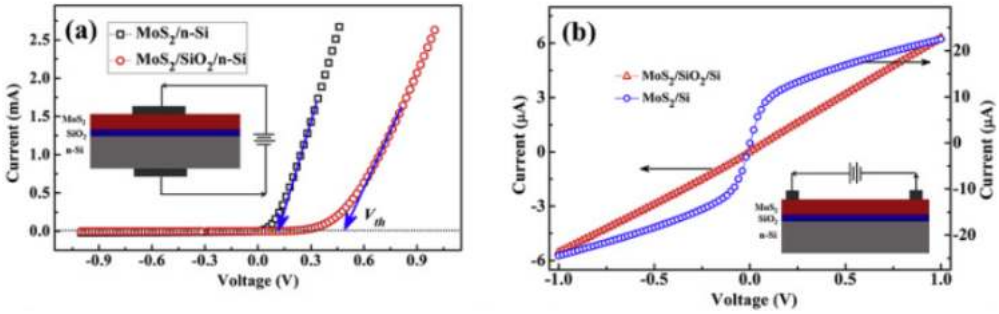

Figure 1.6: Position voltage dependence for vertical (left) and lateral (right) [4]

1.3.1 Contributions

The work of this thesis continued the photo-electric characterization of asymmetrical MoS_2 devices using transient analyses. How the transient response changes across the devices active area are a primary focus of this thesis. Two asymmetrical devices built-in electric fields were measured and compared via their respective contact geometry ratios and com-

pared to literature. The position and charge density dependence of carrier lifetimes were determined for a primary device (DUT5) to gain insight into the effects of asymmetric geometry on carrier lifetimes. All experiments were done using a focused laser, with a spot size smaller than the active area of the device, to generate spatially localized photo-carriers. The transient response of the laser blast was measured using an oscilloscope. By employing Transient Photovoltage (TPV) and Transient Photocurrent (TPC) methods and analyses, the position-dependent carrier lifetimes of a device, the charge densities, and the built-in electric fields of two devices were all determined. These findings will allow informed decisions to be made on device sizing, and assist in determining appropriate applications for these devices. Whereas the carrier drift mobilities were unable to be determined due to time constraints.

1.3.2 Thesis Organization

This thesis is divided into 4 chapters. The first chapter is an overview of photovoltaic nano structures and asymmetrical MoS_2 devices. The second chapter covers the experimental procedure and setups, and provides an overview of each device studied. The third chapter covers the analysis and results gathered from the experiments and compares the devices against each other and and to literature, as well as a discussion of properties, errors, and inconclusive results. Chapter 4 is a conclusion of the thesis, summarizing the key findings, challenges, and future work of this thesis.

Chapter 2

Methods

2.1 Equipment and Laboratory Setup

Devices were optically probed using a Horiba Scientific Delta Diode Picosecond Laser (DL), characterized by a 100-picosecond pulse width with a 1 μm spot size, a 477 nm wavelength, and an average power of 3 mW per pulse. This laser was used to locally excite electrons that resulted in the transient amplitudes. Initially, devices were going to be probed by a single pulse from this laser but every device that was tested failed to respond to a single pulse from the DL. A transimpedance amplifier was employed to detect the signal from a single pulse, but the signal was altered depending on a variety of amplifier settings and so was abandoned in the setup. To adjust to the challenge, a Tektronix AFG3151C Arbitrary Function Generator (AFG) was connected to the DLs controller trigger input. This increased the control over how many consecutive pulses were fired from the DL over an interval, called a "burst", and the length of the interval between firing the next burst. Bursts of 50,000 pulses at 50MHz were used, resulting in an effective pulse duration of 1 ms. For some tests, 10,000 and 1,000 pulses were utilized, producing bursts of 100μs and 20μs, respectively. This setup was expected to alter the rise time of the transients, which restricted the analysis of the transients to exclude any rise times. The current-voltage (I-V) characteristics and open circuit voltage (V_{OC}) measurements were done with a Keithley 2400 source-meter, with the small area contact always connected to ground. The Keithley 2400 was also used as the bias voltage power supply for the electric field experiments. The transient signals were measured using a Tektronix MDO3404 oscilloscope. To choose the probing location, hence moving the laser spot around on the DUT, was done with a high precision x-y micro-positioning stage.

A second laser was used to provide a uniform bias illumination, which was necessary for varying the V_{OC}, was provided by a 440 nm continuous wave laser with a spot size of roughly 240 μm. This illumination laser was capable of delivering 7.5 $\frac{\text{mW}}{\text{cm}^2}$ but was reduced to 300 $\frac{\mu\text{W}}{\text{cm}^2}$ as the illumination laser was positioned at an angle of roughly 45 degrees above the device under test (DUT). The device illumination, and thus the V_{OC}, was varied using

a graduated neutral density filter (GDF). Each V_{OC} was selected to be approximately 50 mV apart from one another.

Each device was connected to the external measuring circuit in an identical manner. Figure 2.1 illustrates the method of establishing the electrical connection to the device using a probing stage and micro-positioning probes that are contacting the electrodes on substrate. Figure 2.2 depicts the broader setup for the two experimental techniques.

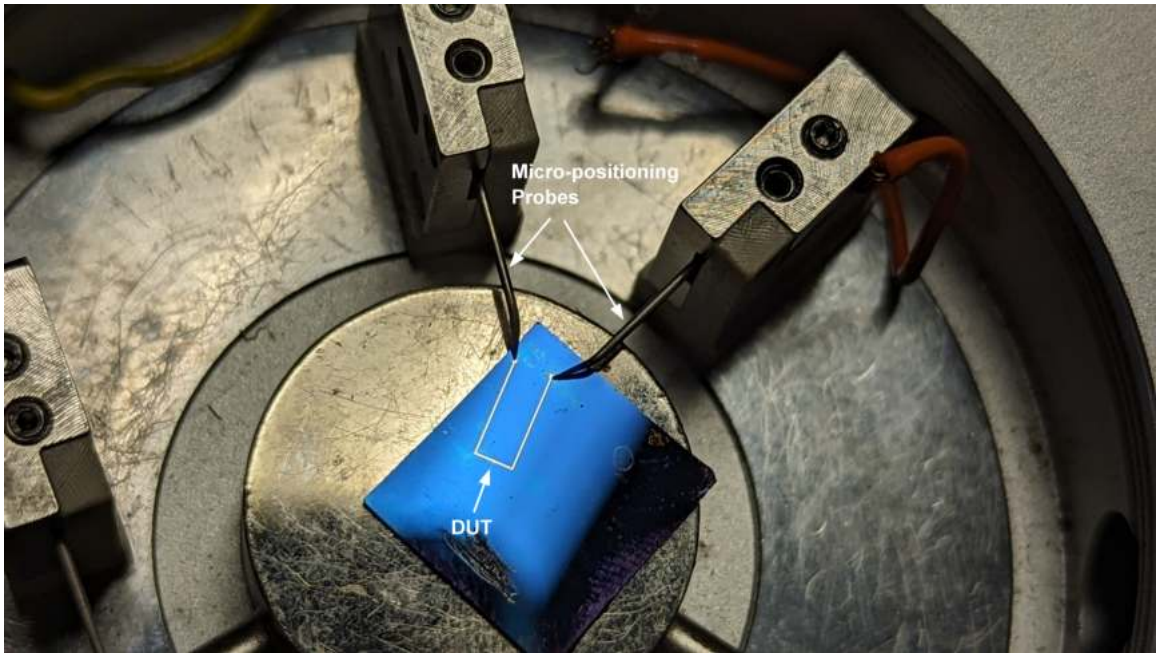

Figure 2.1: Device connected using micro-positioning probes

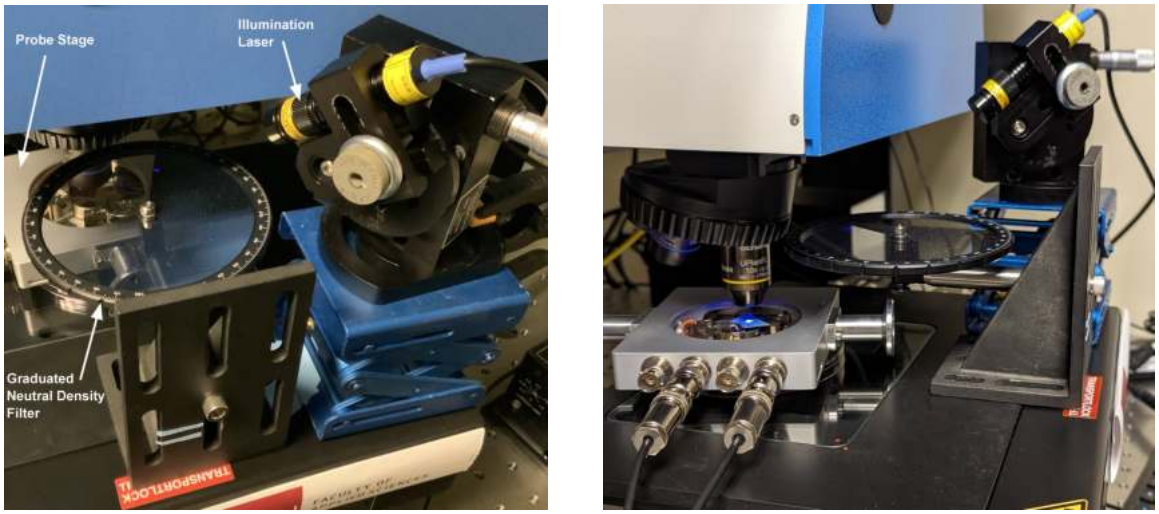

Figure 2.2: Equipment setup with illumination laser and graduated neutral density filter

2.2 Transient Measurements

There are a few options for estimating the carrier lifetimes in solar cell devices with all options being a transient technique. Common techniques include impedance modulated photovoltage spectroscopy, transient photovoltage, open circuit voltage decay and photo luminescence spectroscopy. Each come with certain advantages and disadvantages and decisions one which technique to use requires considerations on available equipment, material, and depth of analysis.

The analysis of the transient behavior in the asymmetrical devices involves two complementary methods: TPV and TPC experiments. These experimental methods are typically performed together due to their similar data gathering approaches, ease of setup, straightforward analytical methods, and less sophisticated equipment demands compared to other transient experiments. However, the analysis proved challenging, as the experiments detailed in this thesis appear to be the first application of TPV and TPC methods for characterizing MoS_2 nano structures. The data gathering process is performed while the device is held at various V_{OC} and in an open circuit configuration for TPV measurements and in a short circuit configuration for TPC measurements, displayed in Figure 2.3. Lastly, conducting TPC experiments with the same set of bias illuminations as the TPV experiments enables the estimation of charge carrier density at various V_{OC}.

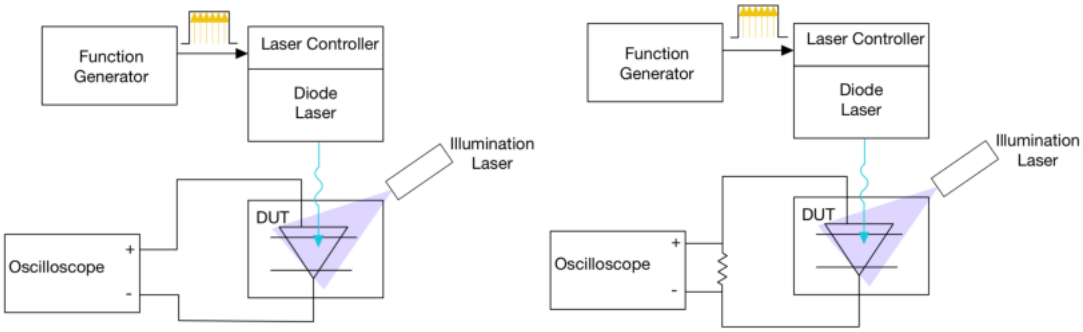

Figure 2.3: Setup diagrams. Left: TPV setup, Right: TPC setup.

Transient Photovoltage Measurements

The TPV method was selected to determine the charge carrier lifetimes of the primary device. In TPV literature, you must ensure the DUT meets certain conditions for accurate analysis. First, the device must be under an appropriate amount of uniform illumination such that the transient voltage amplitude is sufficiently small compared to the V_{OC}. Typically, an appropriate transient voltage amplitude would be less than 20 mV, allowing the increase in transient voltage to be directly proportional to the increase in the carrier density. This condition is necessary for the transient charge carrier kinetics to behave similarly to that of bulk steady state operation and that the TPV decay is mono-exponential [14] [15]. Additionally, the sufficiently small amplitude is essential to ensure that the decay of

the measured signal is from the recombination of carriers in the device and not from other effects, such as capacitive effects from the junctions.

The circuit must be held in an open circuit configuration to ensure that the charges in the device recombine without being extracted or flow through a short circuit meaning that the decay in the transient voltage signal is assumed to be purely from carrier recombination. In TPV literature, the oscilloscopes 1MΩ input impedance is accepted as sufficient to maintain an open circuit for measurements [14].

Each V_{OC} was selected using the illumination laser and GDF as a combined system. The illumination laser was static, with its laser spot illuminating the device while the intensity of the illumination was selected by rotating the GDF to reflect a percentage incoming light off of the DUT, thus controlling the actual incident photon flux on the device. The actual values of the V_{OC} selected for measurements were done in a way that attempted to adhere to the conditions mentioned above and so that a set of measurements across the device were done at V_{OC} that were separated by roughly 50 mV. The process done to complete this was to illuminate the device, measure the V_{OC} on the Keithley 2400, and adjust the V_{OC} using the GDF if the V_{OC} was not desirable for measurement, and then repeated until a desirable V_{OC} was found.

Extraction of the electron lifetimes τ_n was accomplished by curve-fitting the decay profile of the TPV observed across the device. The TPV method relies on a mono-exponential fit of the voltage decay which means that it only can determine the lifetimes of the longest lived charge carriers. The standard mono-exponential TPV equations [16] are derived from the continuity equation and have the form:

$$\Delta V_{OC}(t) = \Delta V e^{-\beta t} \tag{2.1}$$

where β is the decay constant to be determined from the TPV decay curve-fitting, ΔV is the peak transient amplitude, and $\Delta V_{OC}(t)$ is the transient amplitude at time t. The relation to the electron lifetime τ_n is

$$\tau_n = \frac{1}{\beta} \times \frac{k_B T}{q} \tag{2.2}$$

where $\frac{k_B T}{q}$ is the thermal voltage, and τ_n is the electron lifetimes [16].

Transient Photocurrent Measurements

The TPC technique is often paired with the TPV technique because the two experimental setups are similar to one another, and when combining their magical powers can utilize a method known as differential charging (dC) to determine the carrier density for each V_{OC}.

When considering the differential charging analysis it is essential to perform the TPC experiments at the same V_{OC} as the TPV experiments to obtain an accurate prediction of the carrier lifetime dependence on charge density. This information is useful because it shows how carrier lifetimes are effected by illumination intensity allowing the performance to be estimated under certain conditions, like full sun illumination.

The experimental setup of TPC is fundamentally similar to the TPV experiment but the charge is allowed to flow through a relatively low value resistor (R_{TPC}) and the voltage across R_{TPC} is measured using the oscilloscope and converted to a current using Ohms Law (V=IR). The goal of these TPC experiments it to extract the collected charge (Δq) generated by the probing laser (DL in this case) by integrating the transient current response. Doing this will provide us with an estimate of the charge generated at a specific location on the device [5] [16]. The equation for the collected charge is thus:

$$\Delta q = \frac{1}{R_{TPC}} \int_0^t \Delta V(t)\, dt \tag{2.3}$$

where Δq is the collected charge of the current transient, R_{TPC} is the short circuit resistor, and V_{OC}(t) is the voltage amplitude measured on the oscilloscope.

Ideally, TPC measurements are conducted using a 50 Ω resistor to create a short circuit condition; however, in our case, a 94 kΩ was necessary to have a measurable response across the entire device length. The higher resistance value increases the transient rise and decay times, which results in an overestimation in the collected charge. Additionally, since this resistance value is approximately 1/10 of the 1 MΩ input impedance of the oscilloscope, the current divider formula tells us current through the resistor constitutes 90 percent of the total current, resulting in a underestimation in the collected charge. This thesis assumes that neither play a significant role in the results, or roughly cancel each other out.

Lastly, the number of pulses selected for the burst needs to be consistent across all TPC measurements to ensure the calculated collected charge isn't altered by the length of time it takes to fire the number of pulses. The number of pulses need to be the same as the TPV experiments.

2.3 Devices Under Test: Geometries and Properties

2.3.1 Device Preparation

The devices were prepared on p-type silicon substrates, which had oxide thicknesses of 300 nanometers and Au-Cr electrodes contacting the ends of the devices forming the Schottky junctions. Using a microscope, the electrode separation was measured to be between 20 to 21 μm. Each device was connected to the circuit in the same fashion, with the small area electrode connected to ground. The small area electrode was assumed to be the pointed tip of each device and confirmed via the similar diode characteristics seen on the I-V curves in Figures 2.7 and 2.10. Each device had a thickness modulation, evident by the color gradient from the reddish to faded green color change across the device seen in Figures 2.5 and 2.8. Device thickness varied between 30 (reddish) and 60 (greenish) nanometers where it is assumed to be 30 nanometers in reddish regions and 60 nanometers elsewhere.

2.3.2 Probing Locations

Each device had 8 locations probed by the DL along a single line between the electrodes. The chosen coordinate system has the origin, $x = 0$ μm, located along the small area contact and increasing towards the large area contact. The physical separation between probe locations was attempted to be 3 μm but since there was an uncertainty of ± 1 μm in the position of the laser spot on the devices active area, the actual distance between probe locations varies. The distances of the probe locations were measured using ImageJ software.

2.3.3 Dark I-V Characteristics

Measurements of the dark I-V characteristics revealed nonzero V_{OC} in dark conditions for both devices. This property was only observed in thickness modulated devices and not in any devices of uniform thickness. This phenomenon will be referred to as the offset V_{OC} or $V_{OC\ offset}$. The offset V_{OC} was unexpected, as devices with built-in fields usually have an V_{OC} of 0 V in dark conditions. The observed non-zero V_{OC} is believed to arise from the screening effect, an ongoing area of study. The screening effect mechanism suggests that the electric field of the device is exposed to atmosphere, unlike silicon diodes, and so can capture charged or dipole molecules in the air and from thermally generated carriers within the device causing a voltage to build at the electrodes [17]. This explanation is believed to account for a majority of the offset V_{OC}. Both devices had a maximum observed V_{OC} under 1 V, as per expectations given that the highest recorded V_{OC} for an MoS_2 device is 1.02 V [18].

Throughout the course of this project, numerous devices were rendered inoperable during testing, setup, and various experimental stages. Additionally, a number of devices failed to function as anticipated. As a result, Device Under Test 5 (DUT5) and Device Under Test 6 (DUT6) emerged as the primary subjects for analysis in this thesis, having withstood the rigors of the experimental process.

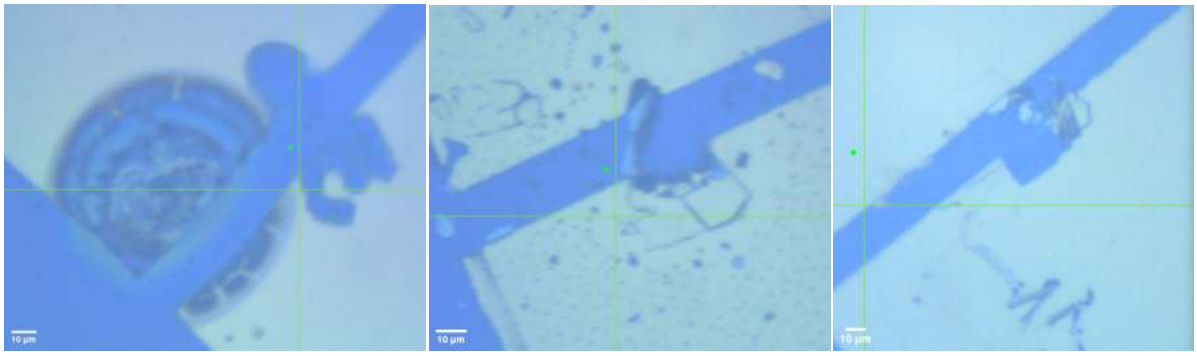

Figure 2.4: Devices destroyed by intense lasing and microprobe scratching

2.3.4 Device Under Test 5

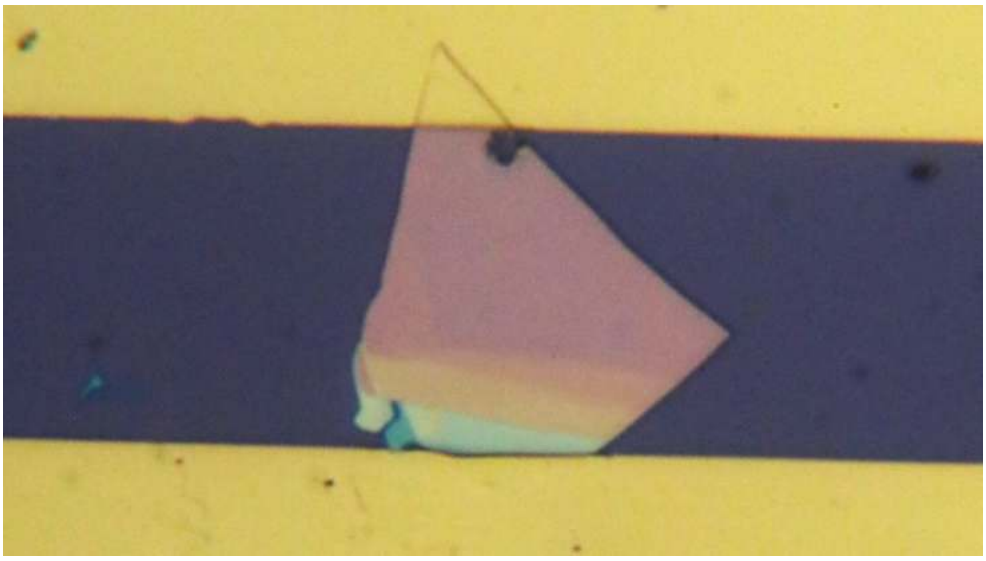

Figure 2.5: Device Under Test 5

DUT5 had a inter-electrode gap of 20 μm and an active area of 312 μm^2. The large area electrode had a contact width of 12.46 μm and a large contact area of roughly 38 μm^2. The small area electrode had a contact width of 5.9 μm and a contact area of roughly 15.7 μm^2, giving the device a contact area ratio of 2.42. The locations that were optically probed by the DL are indicated by the x distances from the origin seen in Figure 2.5. All distance and

area measurements were done with ImageJ software. Given the device area, the maximum incident power on the device was approximately 936 μW from the illumination laser. This was determined from the power density of the illumination laser multiplied by the device active area.

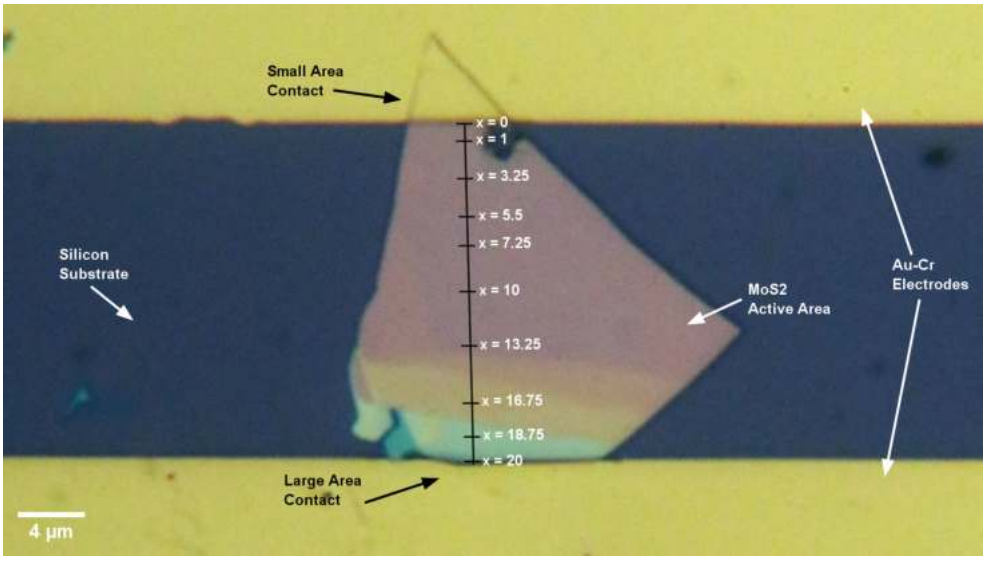

Figure 2.6: DUT5 line of probing spots and distances from the small contact

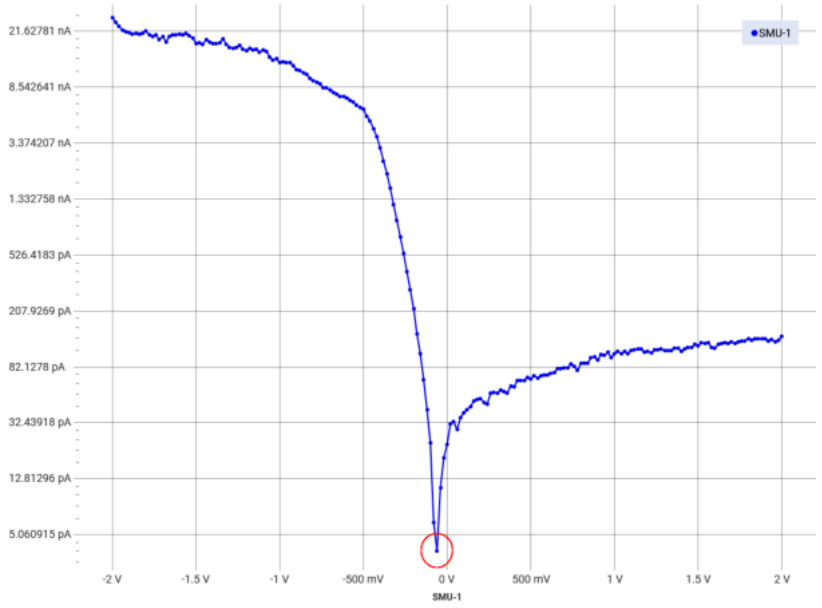

Figure 2.7: DUT5 dark I-V curve. The V_{OC} and dark current are at the same point indicated by the red circle. The value of the $V_{OC\ offset}$ was -70mV

The highest observed V_{OC} for DUT5 was -800 mV, -730 mV after removing the $V_{OC\ offset}$. The dark I-V curve is shown in Figure 2.7. The negative V_{OC} is a result of the connection of the device to the Keithley2400 during measurements, as mentioned above, the small area contact was always connected to ground to be consistent with [3].

2.3.5 Device Under Test 6

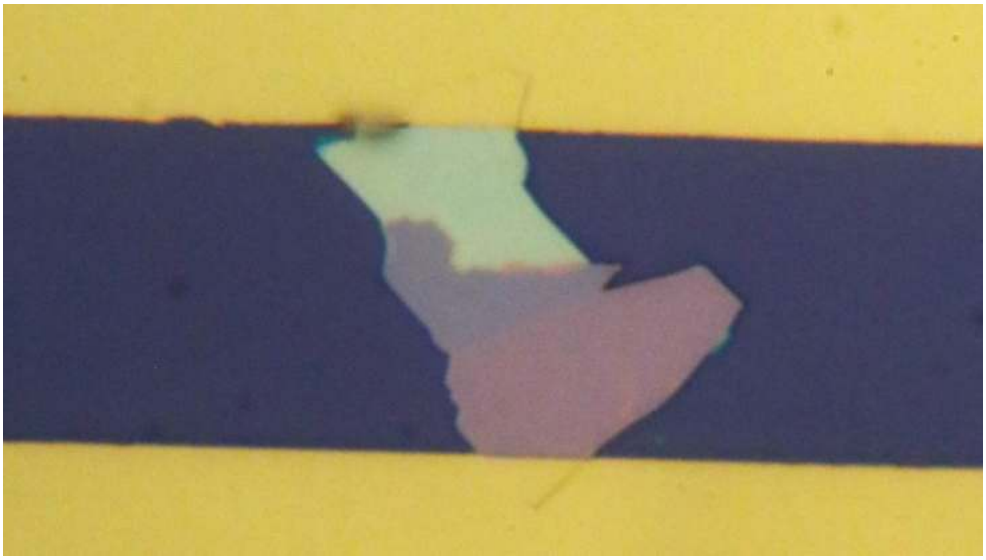

Figure 2.8: Device Under Test 6

This device had a inter-electrode gap of 20 μm and an active area of 274 μm^2. The large area electrode had a contact width of 9.54 μm and a large contact area of roughly 18.92 μm^2. The small area electrode had a contact width of 9.89 μm and a contact area of roughly 10.94 μm^2, giving it a contact area ratio of 1.73. The probing locations depicted in Figure 2.9 are diagonal across the device because the device was oriented to be straight up and down on the screen while taking measurements making it easier to find the same probing location multiple times with less uncertainty. The probed locations are indicated in Figure 2.8 by the distance x from the origin. Given the device area, the maximum incident power on the device was determined to be approximately 822 μW from the illumination laser.

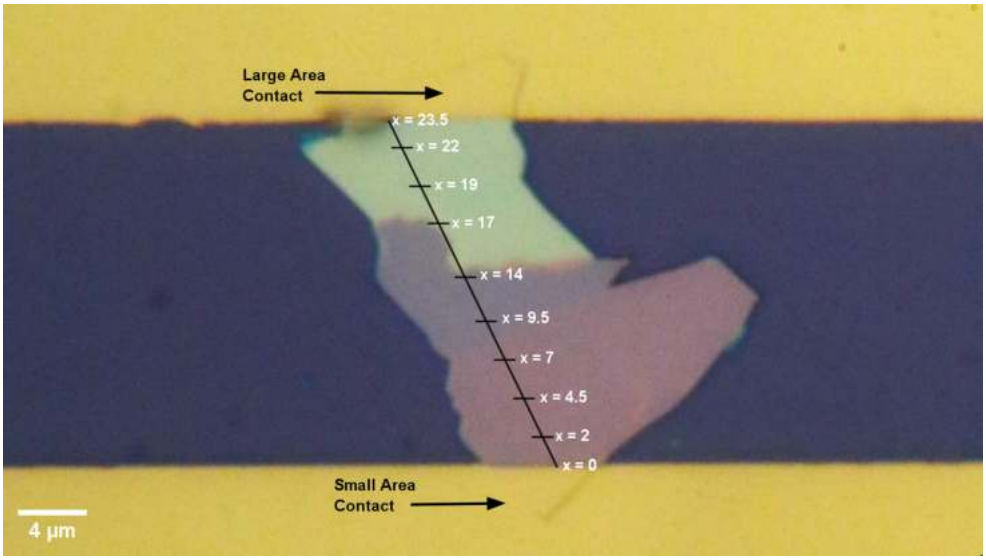

Figure 2.9: DUT6 with the line of probing locations at the x distances

DUT6 had a much larger offset V_{OC} at -380 mV than its counterpart. A possible explanation for the large difference in V_{OC} could be that DUT6 had a much higher light sensitivity than DUT5. Both devices had V_{OC} measurements taken in identical dark conditions; however, it was impossible to completely remove all light from screens and LEDs on equipment from the laboratory environment. This light could have resulted in skewing the V_{OC} of DUT6 during measurement. The largest observed V_{OC} of DUT6 was -588 mV, -208 mV after removing $V_{OC\ offset}$. The dark V_{OC} and dark current are summarized in Figure 2.10.

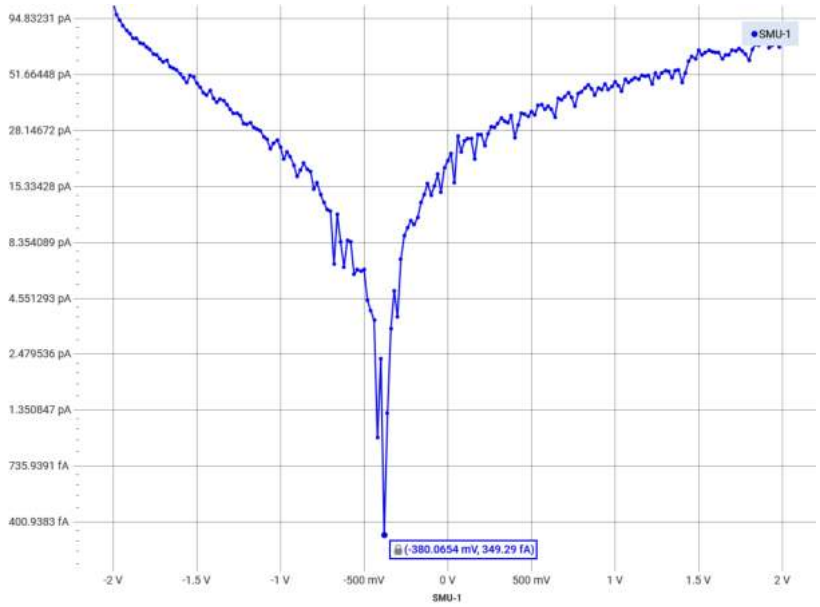

Figure 2.10: DUT6 dark I-V curve depicting the offset open circuit voltage

Chapter 3

Results

3.1 Carrier Lifetimes in Asymmetric Devices

The carrier lifetimes were extracted by applying a mono-exponential curve fit to the transient voltage decay. The fitted decay curve is used to determine the time constant value β in equation (2.2). β must be calculated for each position x at each V_{OC} ($V_{OC\,n}$). Finally, using equations (2.1) and (2.2), the long lived carrier lifetimes are estimated from the time constant.

MATLAB was used to fit each decay curve. To ensure consistency between each fit, the MATLAB algorithm and curve-fitting process were maintained as consistently as possible; however, some areas of the device yielded especially small transient amplitudes. In particular, the center of the device and the area near the smaller contact of the device resulted in smaller amplitudes compared to other areas of the device. Measurements of smaller transient amplitudes lead to noisier data and more uncertain decay constants. For fitted decay curves with especially low signal-to-noise ratios, it was necessary to intervene by modifying the configuration of the MATLAB curve fit to ensure the fit was not critically effected by the noise. An example of the variation in the fitting method can be seen in Figure 3.1.

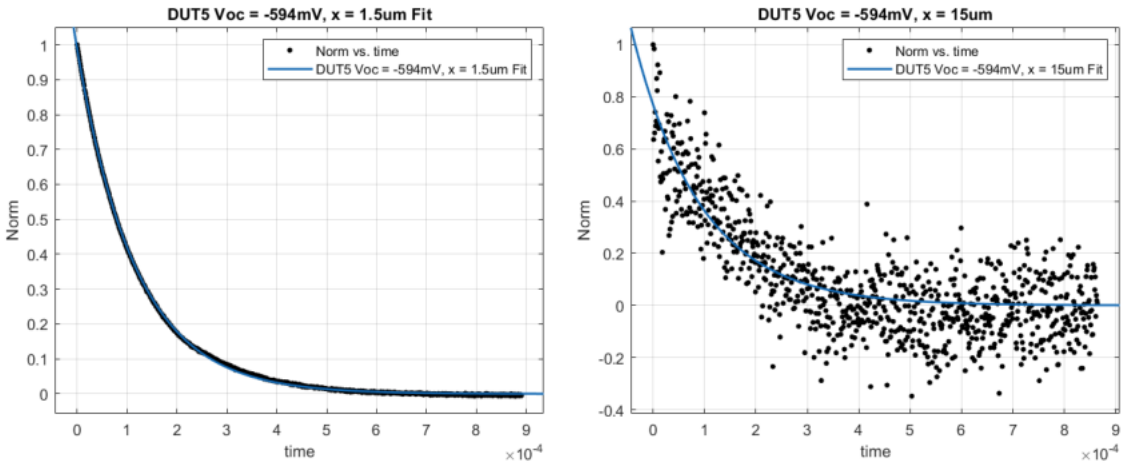

Figure 3.1: Example of variation in fits from MATLAB demonstrating strong SNR (Left) and weak SNR (Right).

One issue with the mono-exponential decay fitting is that its derivations do not assume a lateral transport of the charge carriers. As a result, mono-exponential decay fitting does not account for the recombination that occurs as the carriers drift across the device length to the contact. The amount of recombined carriers would depend on the diffusion length and the built-in electric field of the device. Thus, for probing positions where the charge carriers travel the furthest to reach the contacts, the voltage amplitude measurements and their corresponding decay constant calculations would be skewed.

Further complications develop with the use of the TPV method in maintaining a sufficiently small transient voltage amplitude. The variation in measured amplitudes across the device made it somewhat difficult to adhere to the $\Delta V < 20$ mV condition. This proved especially true for probing locations at the thickest part of the device. On occasion, selecting a sufficiently large V_{OC} for one end of the device made it difficult to measure the amplitude on the other end. As well, selecting a small V_{OC} resulted in the measured transient amplitude to increase beyond the desired 20 mV threshold. Although it was ensured that the variation in probing location was always within the positional uncertainty of 1 μm, the amplitudes of the transient responses were very sensitive to even slight variation in the probing location. This meant that remeasuring the same spot on the device often led to a high variation in the data. In these instances, it was necessary to average measurements in order to have confidence in the TPV and TPC results. Figure 3.2 is an example of the amplitude variation for TPV measurements in DUT5. Note that the plot in Figure 3.2 has the position axis reversed from the one defined in Section 2.3.

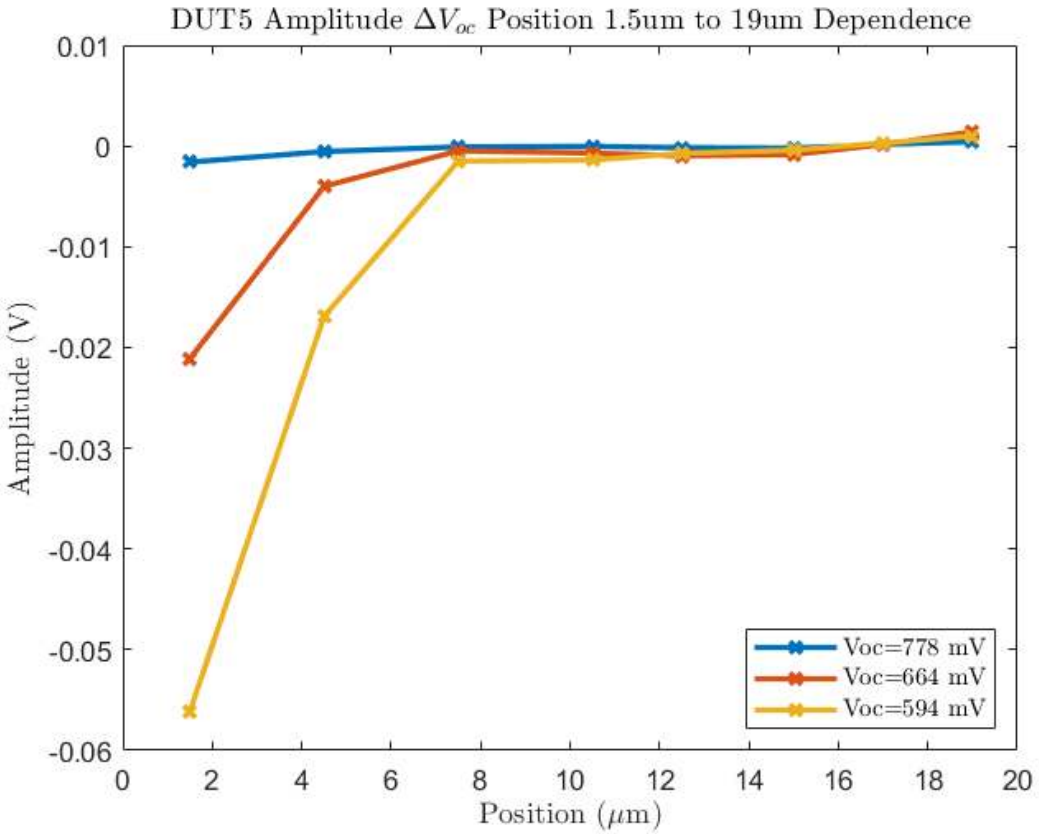

Figure 3.2: DUT5 amplitude variation across the probing line

Interestingly, it was found that for similar selected V_{OC} and similar probing locations on the device, the fitted β values varied more than expected. The V_{OC} data was condensed, averaging data over a 40 mV range (e.g., 530 to 570 mV) of V_{OC} values. This resulted in five V_{OC} values to be used for data analysis. The V_{OC} range was determined so that there were roughly an equal number of β data points in each 40 mV range. The β values are plotted against the V_{OC} in Figure 3.3

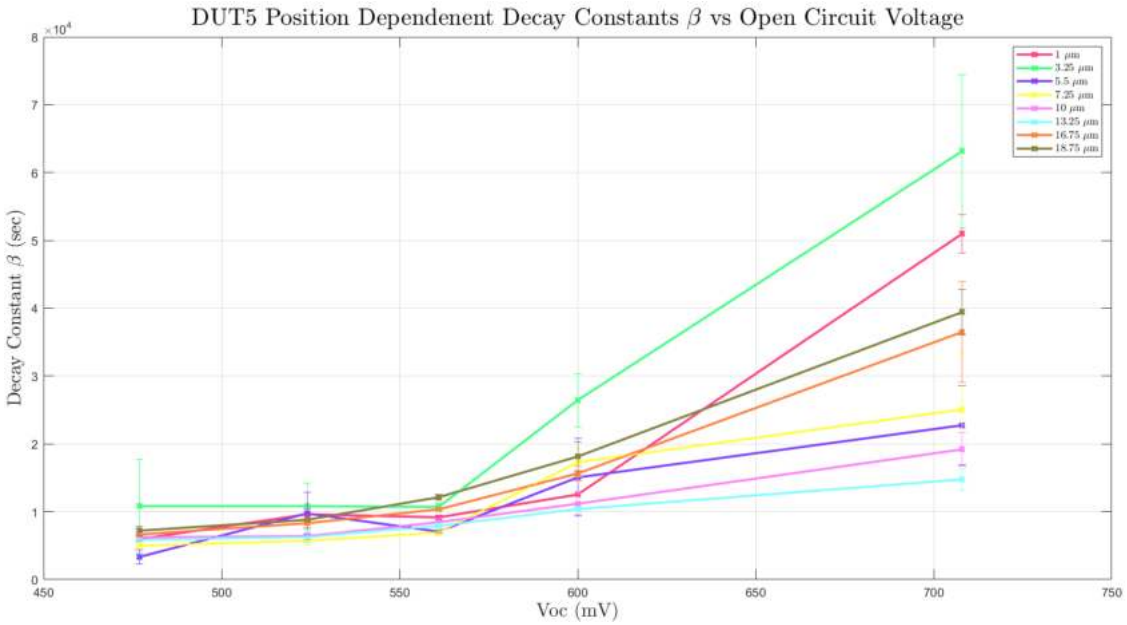

Figure 3.3: DUT5 decay constants across the device

3.1.1 Carrier Density from Differential Charging

Once the decay constants at each position were determined, the charge carrier densities were extracted with the dC method, which utilizes the TPV/TPC synergy. Employing the dC method requires that the TPC measurements are taken at the same V_{OC} as the TPV measurements. $\Delta q_x(V_{OC\ n})$ is the charge collected at position x for a specific $V_{OC\ n}$ indicated by the subscript n. Equation (2.2) for $\Delta q_x(V_{OC\ n})$ is found in section 2.2. Once $\Delta q_x(V_{OC\ n})$ has been found for all x at the nth V_{OC} and the transient voltage amplitudes recorded for the nth V_{OC}, the dC for each position is calculated from:

$$dC_x = \frac{\Delta q_x(V_{OC\ n})}{\Delta V_x(V_{OC\ n})} \tag{3.1}$$

once the dC is calculated for each location (dC_x) and all V_{OC}, one can then determine the total charge produced at a V_{OC} , one location at a time, by integrating the dC_x over all the V_{OC} values used for measurements using equation 3.2:

$$Q_x(V_{OC}) = \int_0^{V_{OC\ n}} dC_x \, dV_{OC} \tag{3.2}$$

where $Q_x(V_{OC})$ is the total charge collected for a single position and a single V_{OC}, and $V_{OC\ n}$ is the limit of integration [14]. This process is then performed for all V_{OC} measured

at each position. A plot of dC vs V_{OC} to visualize the integral can be seen in Figure 3.4 below.

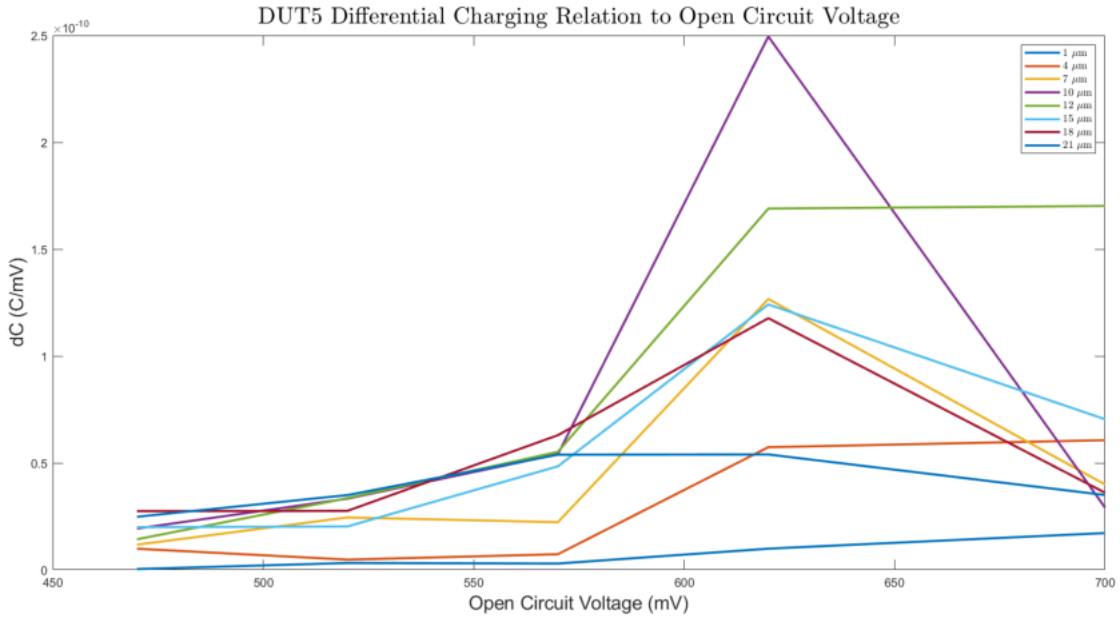

Figure 3.4: DUT5 dC plot for all probing locations

The plot in Figure 3.4 shows how the generated charge at each position is affected by the V_{OC} from the illumination. Where positions 1, 4, and 12 μm are least affected by the V_{OC}. Once the integration is complete, the charge density n_x can be found by dividing $Q_x x(V_{OC})$ by the elementary charge q, thickness d, and contact area A [14].

$$n_x = \frac{Q_x(V_{OC})}{q\ d\ A} \tag{3.3}$$

The thicknesses used were 30 nm for positions (1 to 13.25) μm and 60 nm for positions (16.75 and 18.75) μm. This resulted in charge densities between (10^{12} and 10^{15}) cm^{-3}. These charge densities are similar to other reported charge densities [19] [20], but are a few magnitudes lower as both report in the $10^{17} cm^{-3}$ range, while another source reports the charge densities of in the magnitude of 10^{15} cm^{-3} [21]. The relation between charge densities and carrier lifetimes is summarized in Figure 3.5.

Table 3.1: Mos_2 carrier lifetime comparisons from various sources

Mos_2 Carrier Lifetimes					
	This Work	[23] 1 Layer	[23] 10 Layer	[24] Bulk	[25] bulk
τ	400 - 4500 ns	50 ps	1 ns	200 ps	2.6 ns

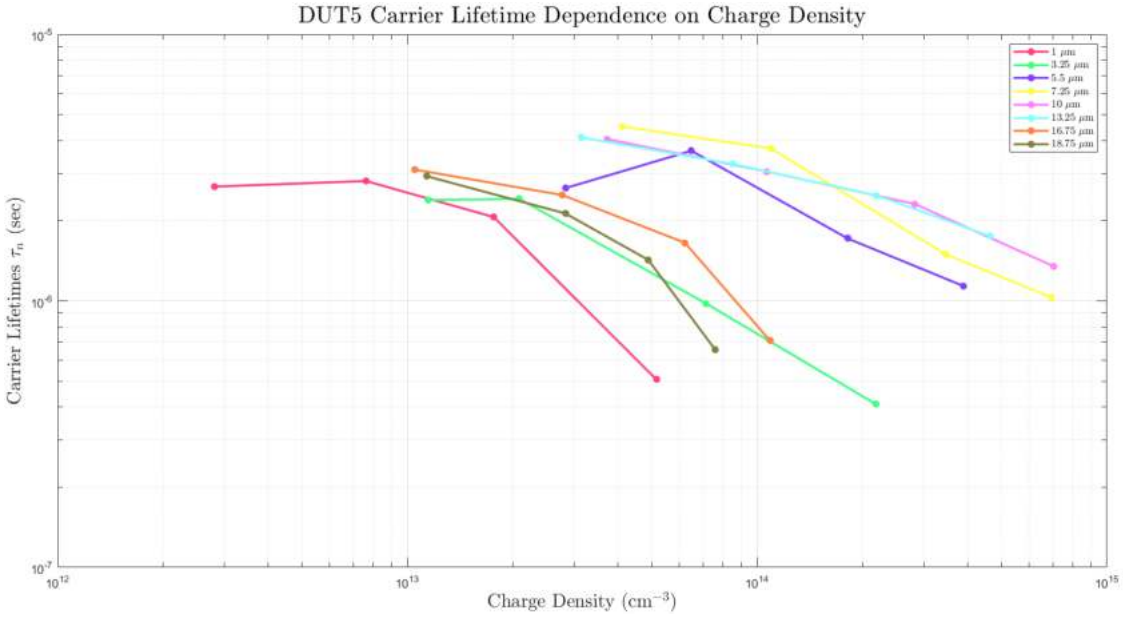

Figure 3.5: Device Under Test 5 lifetime dependence on charge density at probed positions

A notable trend can be seen where the carrier lifetimes decrease as the charge density increases. This relationship between carrier lifetimes and charge density is characteristic of many types of solar cells [22]. Further, a stark difference can be seen between carrier lifetimes near the electrodes and those near the device's center. It is suspected that the lifetimes near the contacts of the device are shorter due to the increase in strength of the electric field near the contacts. Additionally, the relatively large thickness of the device near its large contact allows for a higher number of trap states and recombination centers, which may contribute to the shorter lifetimes. In contrast, the center of the device has a weaker electric field and thus the carriers have a lower drift velocity. Due to the lower drift velocity, the carriers near the center of the device experience relatively slower recombination and therefore larger lifetimes.

3.2 Internal Electric Field of Asymmetrical Devices

Estimation of the built-in electric field required a second round of TPC measurements across the probing locations while applying a variety of bias voltages. DUT5 and DUT6 were both under uniform illuminated and held at a V_{OC} of -0.69 V and -0.18 V respectively. By plotting the charge collected from the current transient against the applied bias voltage,

the built-in voltage at position x can be determined. When plotting Δq_x vs V_{bias} a linear region can be seen for small voltages around 0 V. A linear curve fit of this region can be used to estimate the built-in voltage of the device at x. By extrapolating the linear fit to the x axis intercept, the estimation of the built-in voltage is the resulting intercept value. This plotting method is known as a Hecht plot [5].

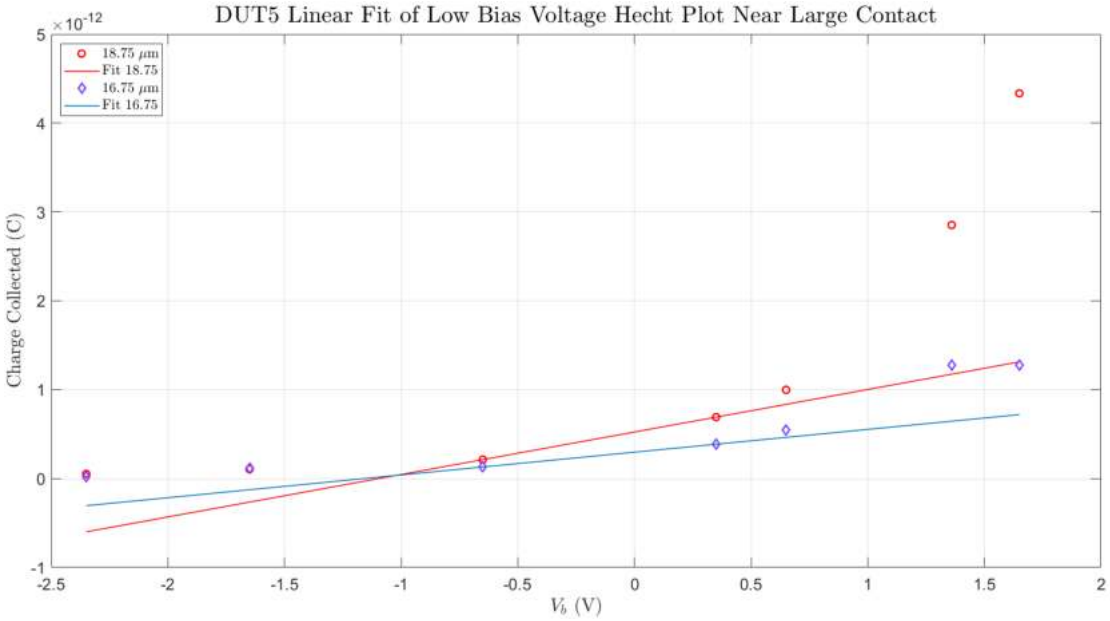

Figure 3.6: DUT5 Hecht plot for two locations closest to the large contact

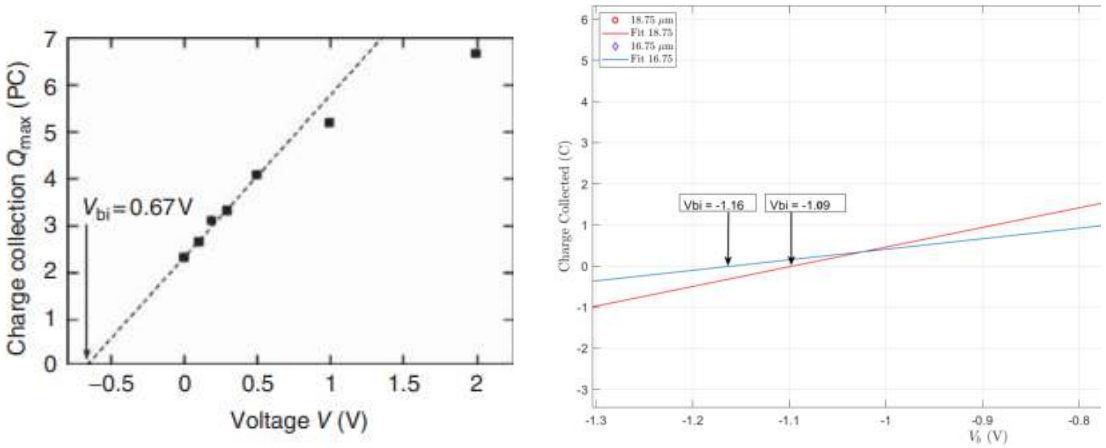

Figure 3.7: Left: Hecht plot demonstrating the extrapolation of the built-in potential [5]. Right: DUT5 Hecht plot indicating built-in voltages

Once the built-in voltage is determined for each position, the electric field is estimated by by dividing the V_{bi} by the distance from the probing position to the contact. The polarity of the response determines which contact on the device should be used for the distance

measurement. Negative polarity indicated that electrons were moving toward the large area contact and vise versa. The electric field estimations for DUT5 and DUT6 are shown in the figures below.

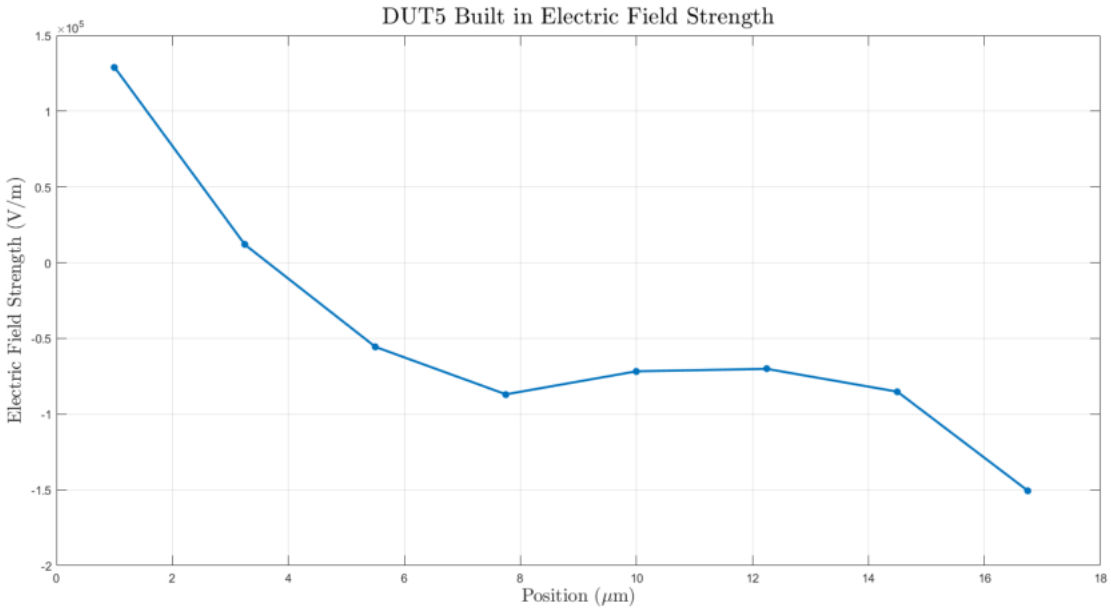

Figure 3.8: DUT5 estimated electric field strength

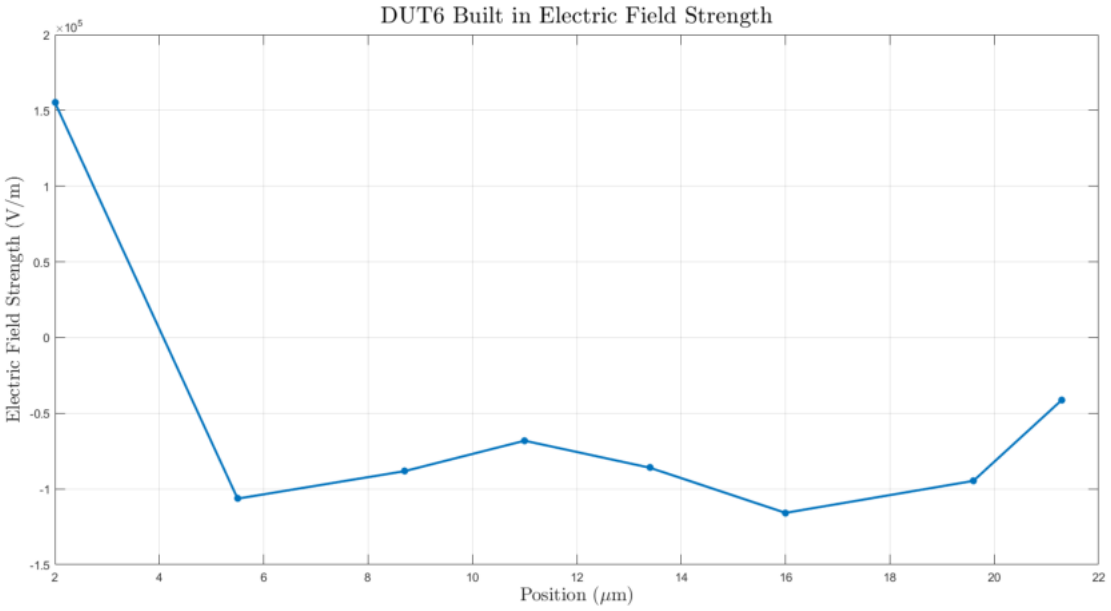

Figure 3.9: DUT6 estimated electric field strength

The electric field strength of both devices peak around $1.5{\times}10^5 \frac{\mathrm{V}}{\mathrm{m}}$ near the small area contact, but differ near their large area contacts. DUT5 and DUT6 have their respective contact asymmetry ratios of 2.42 and 1.73, which may have an effect on the behaviour of the electric

field near the large contact. We attempt to compare the contact asymmetry to the built-in electric field with hopes to assist in the design process of these new MoS_2 diodes but two devices is not enough data for concrete conclusions to be drawn about the relationship between the contact areas, thicknesses, and the electric field so a third device is presented with the hope to assist in the analysis.

3.2.1 Electric Field Comparison

We now compare the results of this thesis to a paper that has simulated an asymmetric WeS_2 device and the respective built-in electric field using COMSOL software and finite element modelling (FEM) which is presented in Figure 3.10. The simulated WeS_2 device was truly 2D with contact widths (not areas), of 5 μm and 0.5 μm, with an inter-electrode gap of 2 μm and Au-Ni contacts. A reminder of the device dimensions studied in this thesis; devices had an inter-electrode gap of 20 μm with large and small contact widths of 12.46 μm and 5.9 μm for DUT5, and 9.54 μm and 9.89 μm for DUT6. The simulated built-in electric field was reported to have a maximum electric field strength of $4{\times}10^6 \frac{\mathrm{V}}{\mathrm{m}}$, roughly one magnitude larger. Considering the difference in the simulated device dimensions and materials used, the results of the simulation agree nicely with the results of this thesis. The strength of the simulated electric field would be higher than the devices measured here because the simulated device is much more asymmetrical with a contact width ratio of 10, versus the width ratios of 2.11 and 0.96 for DUT5 and DUT6 respectively. Given that the asymmetry affects the Schottky barrier heights and the difference in these heights affects the electric field induced, the asymmetric MoS_2 devices may perform even better than WeS_2 at the same asymmetry ratio. The shape of the electric fields for the simulated device and DUT5 are quite similar as well, whereas in DUT6, the similarities stop near the large area contact. This discrepancy in the shape in the field must be caused by the smaller contact ratio, where at a contact area ratio of 1, the shape of the electric field would be symmetric about the center of the device.

3.3 Discussion

3.3.1 Lifetimes

Many sources have indicated that the carrier lifetimes found for MoS_2 are between tens of picoseconds and tens or hundreds of nanoseconds [23] [24] [25]. In this paper, the lifetimes have been measured in the microseconds, with the shortest carrier lifetime at about 400 nanoseconds. Since this is the first occurrence of an asymmetrical MoS_2 device having its lifetimes estimated via TPV measurements, it is understandable that they not agree. The first possibility for the magnitudes difference in lifetimes is that the TPV method was men-

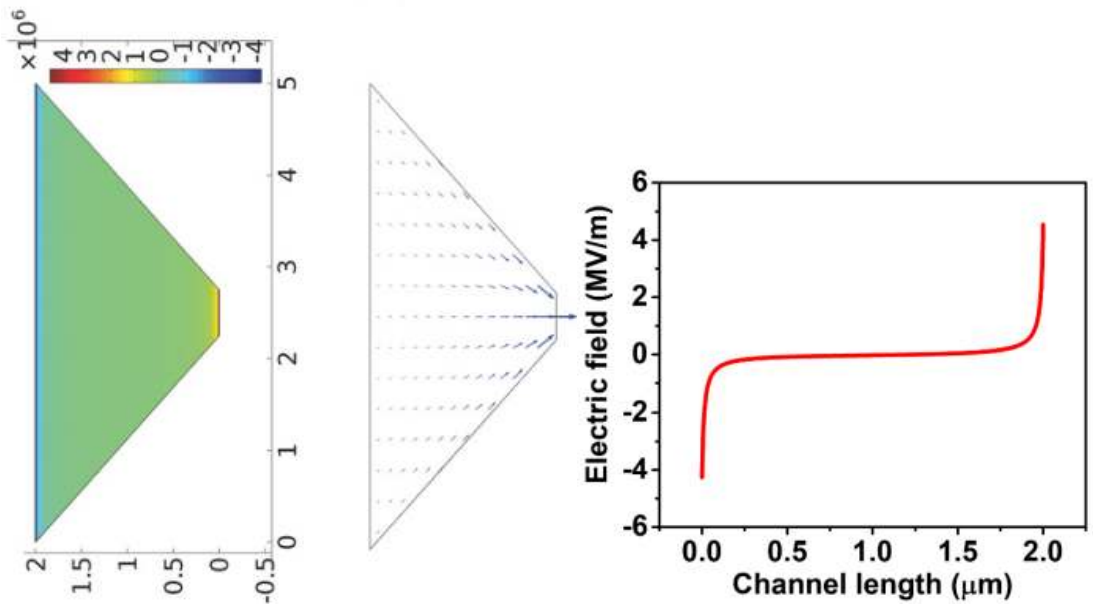

(a) Simulated asymmetrical WeS_2 structure with color indicated electric field strength

(b) Simulated electric field across channel width of (a)

Figure 3.10: COMSOL simulation of WeS_2 device. Reproduced with permission from [6], Wiley Materials 2018.

tioned to only detect the longest lived carrier lifetimes due to the mono-exponential decay. Given that the compared papers are measuring lifetimes through different methods could account for the wide discrepancy in the reported carrier lifetimes. A distinction between the methods of the compared papers and this thesis is in many papers the carrier lifetimes that are measured are either radiative recombination lifetimes or exciton lifetimes for monolayer MoS_2. Radiative recombination lifetimes and exciton lifetimes are similar and occur when an electron-hole pair created from the same photon absorption event recombine with each other after a short time. Radiative recombination requires a monolayer for measurements because it measures the photoluminescence, which requires the direct bandgap of monolayer MoS_2. Excitons are a type of dual charge carrier, bounded together by the coulombic force when electrons and holes are not separated by some mechanism, like an electric field.

Another possible explanation could be the difference in thickness of the asymmetric MoS_2 investigated in this thesis and the thicknesses in the compared papers. Most sources have investigated the lifetimes of monolayer MoS_2 while this thesis investigated 30 to 60 nm MoS_2. This difference in thickness could account for some of the discrepancy in the results as the carrier lifetimes were shown to increase by two magnitudes from 40 ps to 1 ns by increasing the number of MoS_2 layers from 1 to 10 [23]; however, it is not clear whether this trend for thickness dependence on carrier lifetimes would continue up to the thickness of 30 to 60 nm, or 38 to 75 layers thick.

A last possibility in the discrepancy of results is that the experimental design used in this thesis was flawed and overlooked some factor that resulted in measuring the voltage decay of the discharging electrodes instead of the decay of the MoS2 photovoltage. This could be possible if the RC of the external circuit rivals the junction capacitance and shunt resistance ($R_{sh}C_o$) of the device [26]. However, the experimental setup was confirmed using a Thorlabs DET10A silicon photodetector where a single pulse response was measured. With TPV still being widely used to study pervoskite, silicon, and organic solar cells, combined with the simplicity of the experimental setup, it is difficult to imagine that others measure recombination lifetimes using this method if the measurements can easily be disrupted by the external measurement circuit. On the other hand MoS_2 and specifically asymmetrical MoS_2 are unlike any other solar cells previously studied using the TPV and TPC methods. Certainly these results would need to be confirmed by future experiments to better understand the nature of these papers results and the results of this thesis. If this papers results are accurate, then asymmetrical MoS_2 is a simple and easy way of fabrication that increases carrier lifetimes by roughly 100 to 1000 times, better than any surface treatment used to increase carrier lifetimes.

3.3.2 Built-in Electric Fields

When observing the built-in electric field plots of each device, there is a noticeable similarity to plots of the device's photovoltage amplitudes. With this similarity in mind, determining if there is a simple relationship between the TPV amplitude and the electric field could assist in developing a method for electric field estimation purely from the transient photovoltage amplitude, contact asymmetry, and thickness. The plots of amplitudes and electric fields for each device are presented in Figure 3.11 and 3.12 below to show these similarities. A last observation is the large contact side, $x = 21$, of DUT6 doesn't drop further in the negative as seen in DUT5, and the reported device.

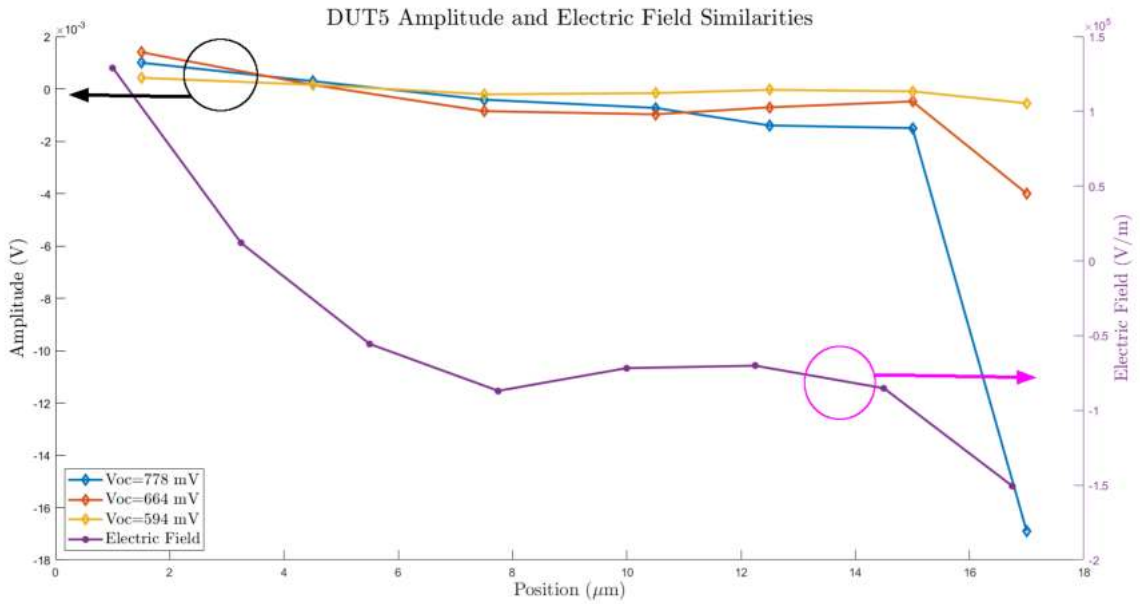

Figure 3.11: DUT5 amplitude and electric field similarities

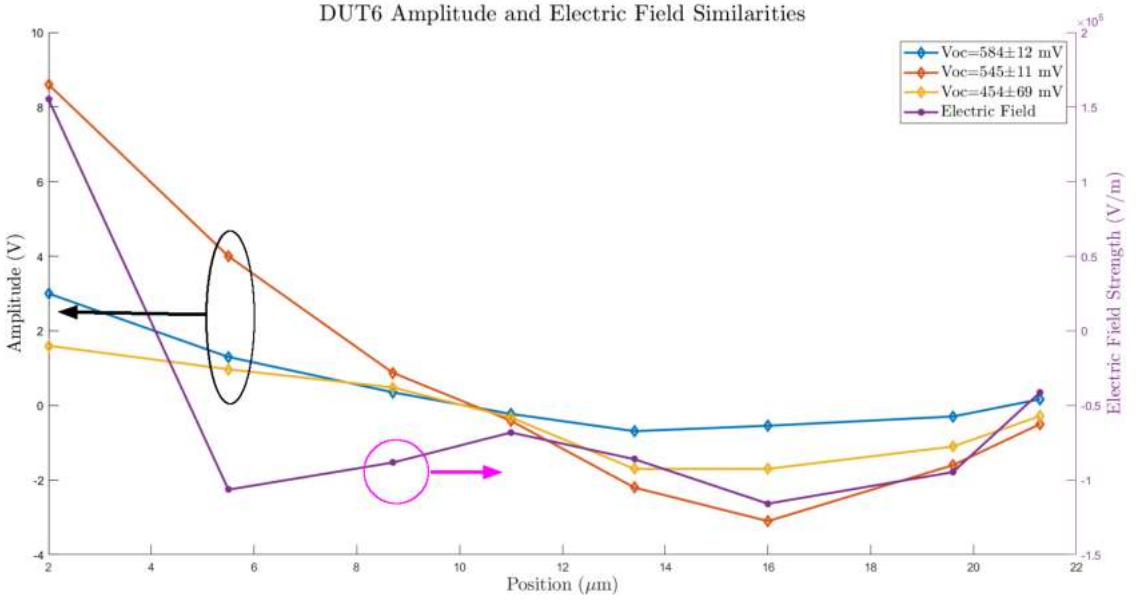

Figure 3.12: DUT6 amplitude and electric field similarities

Chapter 4

Conclusion

4.1 Thesis Shortcomings

The primary limitation of this thesis lies in the inability to verify its results without future experimentation, marking a significant area of disagreement. The possible explanations are that the TPV method cannot be used for this material for reasons that are unknown, the external measurement circuit measured something other than the carrier lifetimes of the MoS_2, or the asymmetrical geometry increases the carrier lifetimes to be in the microsecond range.
Another limitation of this thesis was the lack of MoS_2 devices studied and analysed. Only two asymmetrical devices could be studied, with only one device having the charge carrier lifetimes and charge densities determined. The absence of an adequate comparison between asymmetrical and symmetrical devices leaves a lot to be questioned about the asymmetrical device performance since there is no baseline performance of the symmetrical device. Symmetrical devices where studied briefly, but were rendered inoperable before experimentation was complete, or were determined to be a bad device to use for a comparison due to poor Au-Cr electrode quality.

4.2 Uncertainties

The uncertainties and potential errors are reviewed in this thesis in detail. There are 3 main subsections concluding uncertainties.

4.2.1 Diode Laser Spotsize

The focus of the laser was not constant throughout the measurements; it drifted, slowly increasing the spot size over time. This drift would result in more generated carriers and, as mentioned above, the amplitude of the voltage response was quite sensitive to changes in location over the active area of the device. Consequently, these effects would likely increase the calculated charge density.

4.2.2 Probing Location

To focus the DL required the defocusing of the microscope that was used to visually position the DL over the device. This defocusing led to a greater uncertainty in the DL probing location across the device. The uncertainty from the blurred device on screen combined with the physical orientation of the device not always being perpendicular on the screen led to uncertainties in probing location. This uncertainty was mitigated as much as possible by taking photos of the probing location using a smartphone, but the lack of detail on the device made relocating the exact same probing spot more difficult.

4.2.3 Equipment

The measuring equipment (oscilloscope and Keithley 2400) added measurement uncertainties to the data. The V_{OC} measured by the Keithley2400 varied by ± 10 mV during repeat measurements. The oscilloscope consistently had noisy oscillations that were apparent at very small signals leading to greater uncertainty of the small amplitude locations. This small signal-to-noise ratio was, at times, difficult to handle with the MATLAB algorithm when curve-fitting.

4.3 Future Work

Future work should be primarily focused in refining the measurement method of determining the built-in electric fields for more devices and confirming the built-in fields of DUT5 and DUT6 using a simulated approach. A simulation using COMSOL would be the fasted way to validate the strengths of the built-in electric fields of DUT5 and DUT6 while providing a foundation to confirm future results. Understanding the relationship between the contact asymmetry and the electric field could open up applications for finely tuned geometry, as is the case for silicon photodiodes.

4.4 Concluding Statements

In this thesis, the effective carrier lifetimes were measured using the TPV technique and were determined to be between 500 nanoseconds and 6 microseconds. The carrier lifetimes showed device-position dependent qualities and typical behavior when plotted against the charge density, which lends some validity to these results. The combination TPV and TPC measurements resulted in charge densities within the same expected magnitudes for MoS_2. Lastly, the built-in electric field was estimated to be 150 kV/m at the electrodes, and were in the same realm as the compared WeS_2 device considering the contact asymmetry. Future work should continue focusing on the relationship between built-in electric fields and contact asymmetry, as well as verify the lifetimes via other means. If the built-in field can separate

the charge carriers effectively enough to increase the lifetimes by magnitudes, the MoS_2 will have far more potential applications than initially thought.

Chapter 5

Appendices

5.1 Devices Under Laser Microscope

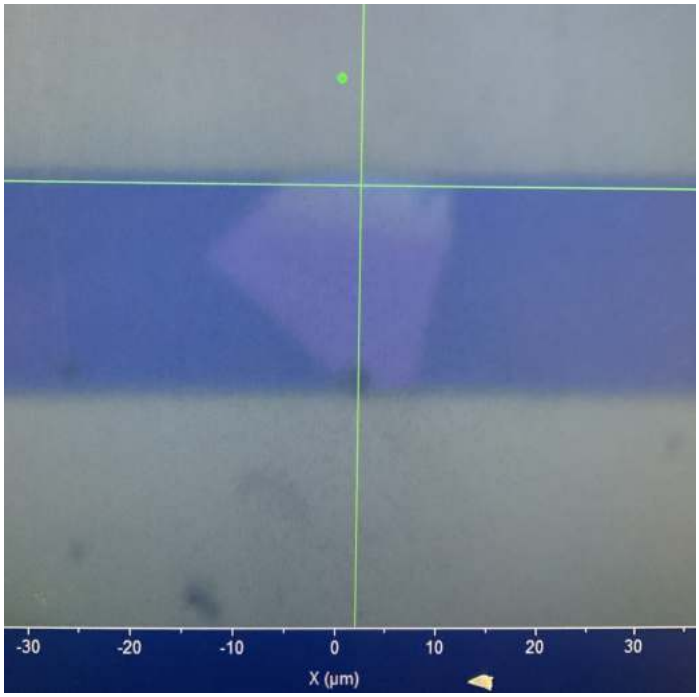

Figure 5.1: DUT5 in focus under microscope

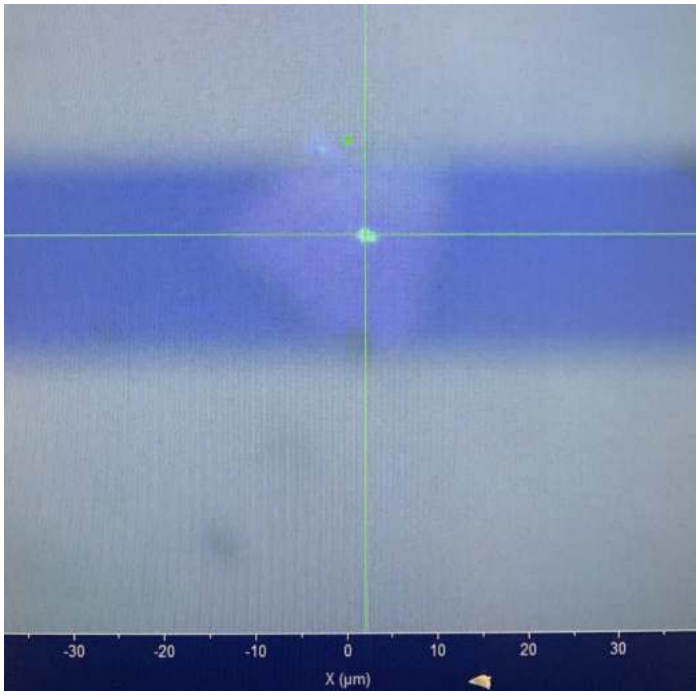

Figure 5.2: DUT5 out of focus under microscope show laser location uncertainty

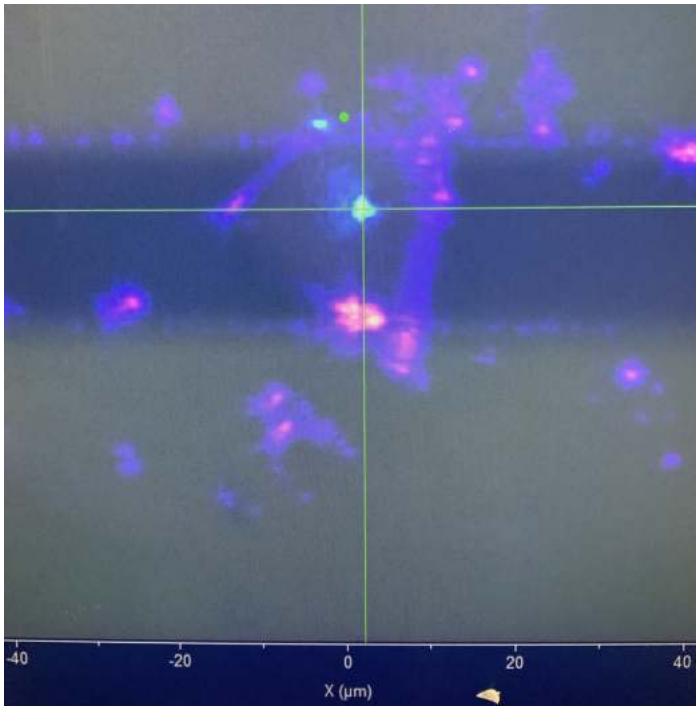

Figure 5.3: DUT5 under illumination by illumination laser

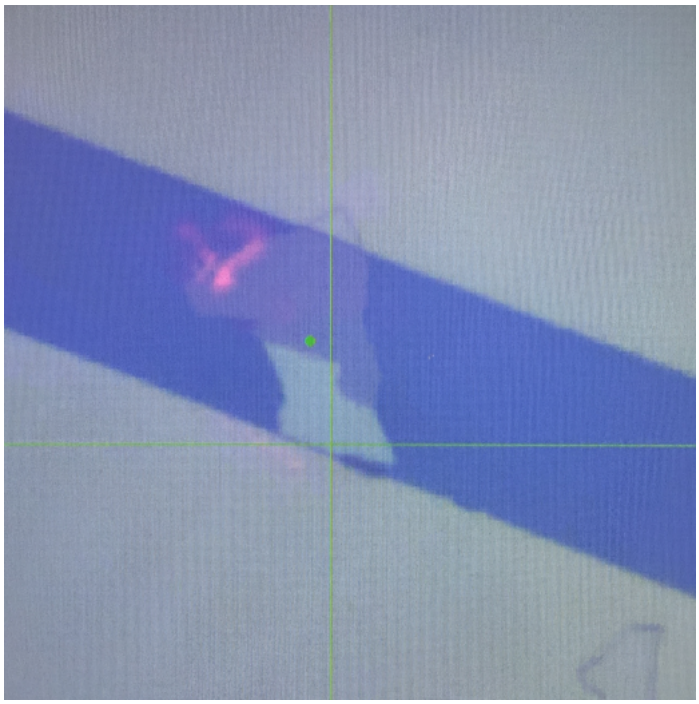

Figure 5.4: DUT6 oriented perpendicular to screen resulting in a diagonal line seen in section 2.3.5

5.2 MATLAB Algorithms

5.2.1 TPV Processing

```
NegResp = false;
 if exist('ANALOG','var') == 1
    laserON = ANALOG(18:length(ANALOG)-1,:);
    Response = VarName3(18:length(VarName3)-1,:);
    time = WaveformType(18:length(WaveformType)-1,:);
 end
laserON = round(laserON);
LightON = find(laserON==1);
LightON_Indx = LightON(2); %Start of laser burst
LightOFF_Indx = LightON(end); %End of laser burst
Response1 = Response(LightOFF_Indx+1:round(length(time)*(10/10))); %Shorten Array to isolate response
time1 = time(LightOFF_Indx+1:round(length(time)*(10/10)));
time1 = time1 - time1(1); % Burst start is t = 0
Response2 = Response1 - mean(Response1(round(length(Response1)*(3/4)):round(length(Response1)*(11/11))));% shift response to decay to 0
Response2 = Response2./abs(mean(Response2(1:10))); % Normalize
% Response2 = Response2./abs(max(Response2));

%Moving average od data for noisy or high data signals
M = movmean(Response1,5);
T = movmean(time1,5);
if length(Response)>=10000 % Average out the waveform a bit

    for i=1:length(Response1)*0.5000
        M = movmean(M,5);
        T = movmean(T,5);
    end
end

% Invert response if negative, flag to keep true response
if Response(LightOFF_Indx-10)<0
    Response2 = -1.*Response2;
    M = -1.*M;
    NegResp = true;
end

% Further Isolate the response
% This part usually required a personal touch
Min_valu = min(M);
Decay_end_Indx = find(M==Min_valu);
% Response1 = Response1(1:Decay_end_Indx);
% time1 = time1(1:Decay_end_Indx);
% M = M(1:Decay_end_Indx) - M(Decay_end_Indx);
% T = T(1:Decay_end_Indx)- T(1);
M = M - (M(end)+M(Decay_end_Indx))/2; %round(length(M)/2)  (M(end)+M(Decay_end_Indx))/2 (abs(max(M(Decay_end_Indx:end)))-abs(min(M(Decay_end_Indx:end))))/2
% Response2 = Response2(3750:18200) - Response2(18200);
% time1 = time1(3750:18200) - time1(1);
```

```
Norm = M./max(M(1:5));S
%%%%%%%%% ADDED Nov 15 %%%%%%%%%%%%%
%%%% Conduction Band Lifetime estimation%%% Not Used
% lifetimes should be within 1 and 100 ns to agree with litureature
% Set k_cb to be 1 to 100 ns and determine Nt0, or n_eq, or NC
% v(t) =
% -(kBT/(q-(TC/T))ln[t*k_cb*(1-(T/TC))(NC*TC/(Nt0*T))(n_eq/NC)^(1-T/TC)]
T = 300;
kB = 1.3792E-23;
e_charge = 1.6E-19;
TC = 515; %Characteristic temp of MoS2
NC = 1.5E15; %cm^-3
Nt0 = 1E18;
n_eq = 1E13;

% C0 = kB*T/(e_charge*(1-(T/TC)));
C0 = kB*T/(e_charge*(1-(T/TC)));
C1 = exp(((T/TC)-1)*e_charge*max(M)/(kB*T));
C2 = (1-(T/TC))*((NC*TC)/(Nt0*T))*((n_eq/NC)^(1-(T/TC)))*time1(round(0.2*length(time1)));
k_cb = (exp(Response2(round(0.2*length(time1)))/C0))/C2
k_cb = 1/k_cb
%%%%%%%%%%%%%%%%%%%%%%%%%%%%%%%%%%%%%%%%%%%%%%%%%%%%%%%%%%%%%%%%
% PLOTS

% figure;
% semilogx(T,Norm)
% title('DUT5 TPV Response Semilog $\beta$','Interpreter','latex');
% xlabel('Time (sec)','Interpreter','latex');
% ylabel('Decay Constant $\beta$','Interpreter','latex');
% % legend('x = 1 ($\mu$m)','x = 4 ($\mu$m)','x = 7 ($\mu$m)','x = 10 ($\mu$m)', 'Interpreter','latex');
% grid on
% hold on
% figure;

% semilogx(time1,Response2)
% title('DUT5 TPV Response Semilog $\beta$','Interpreter','latex');
% xlabel('Time (sec)','Interpreter','latex');
% ylabel('Decay Constant $\beta$','Interpreter','latex');
% legend('x = 1 ($\mu$m)','x = 4 ($\mu$m)','x = 7 ($\mu$m)','x = 10 ($\mu$m)', 'Interpreter','latex');
% grid on
% hold on

tt = log10(time1);
TT = log10(T);
AA = log(Response2);
A = log(Norm);
plot(time1, AA)
```

```
hold on
grid on
title('DUT5 TPV Response Semilog','Interpreter','latex');
xlabel('Time (sec)','Interpreter','latex');
ylabel('Normalized ln($\delta$V)','Interpreter','latex');D

NegResp %Notify if response was <0
P_P = max(M) - min(M) %Peak to peak amplitude estimate
clear ANALOG WaveformType VarName3;
```

5.2.2 TPC Processing

```
R_tpc = 92000; %TPC Resistor
numPulses = 1000;
flag = false; % Set negative response flag
 if exist('ANALOG','var') == 1
    laserON = ANALOG(18:length(ANALOG)-1,:);
    Response = VarName3(18:length(VarName3)-1,:)./R_tpc; %Voltage to current
    time = WaveformType(18:length(WaveformType)-1,:);
    k = k+1; % Array index for automatically filling array with charge collection values
    if mod(k,6) == 0
        k = 1;
    end
    clear ANALOG WaveformType VarName3;
 end
laserON = floor(laserON);
LightON = find(laserON==2); %Sometimes DL pulse amplitude 2 and sometimes 1
if isempty(LightON)
    LightON = find(laserON==1);
end
LightON_Indx = LightON(1);
LightOFF_Indx = LightON(end);
%Response main array
Response1 = Response(LightON_Indx-40:LightON_Indx+(round(length(time)*(2/5))));
time1 = time(LightON_Indx-40:LightON_Indx+(round(length(time)*(2/5))));
% Moving mean for noisy or high data point arrays (0ver 100k points)
M = movmean(Response1,5);
T = movmean(time1,5);
if length(Response)>=10000 % Average out the waveform a bit
    for i=1:round(length(Response1)*0.2000)
        M = movmean(M,5);
        T = movmean(T,5); %,'Endpoints','shrink'
    end
end
% Isolate the response
Min_valu = min(abs(M(round(length(M)/2:end))));
R_min = min(abs(Response1(round(length(Response1)/2:end))));
Decay_end_Indx0 = find(abs(Response1) == R_min);
Decay_end_Indx1 = find(abs(M)==Min_valu);
Response1 = Response1(1:Decay_end_Indx0(end)) - M(Decay_end_Indx1(end));%Response1(Decay_end_Indx0(end));
time1 = time1(1:Decay_end_Indx0(end));
M = M(1:Decay_end_Indx1(end)) - M(Decay_end_Indx1(end));
T = T(1:Decay_end_Indx1(end));
%Charge collection is the integral of current over time
Q_0 = trapz(time1,Response1);
Q_0_arr = cumtrapz(time1,Response1);
Q_1 = trapz(T,M);
% Q_1_arr = cumtrapz(T,M);
```

```
R_tpc = [1000,5000,10000,47000,100000,1000000];
b = [1.583e6,6.68e5,4.241e5,9.427e4,4.756e4,8586];
b1 = b./max(b);
Q0_arr(k) = Q_0; % Fill the arrays for analysis by final program
Q1_arr(k) = Q_1;
```

5.2.3 TPV Processing 2

```
Pos = [1.5, 4.5, 7.5, 10.5, 12.5, 15, 17, 19]; %Position in micrometers
% Pos = transpose(Pos);
% Pos = flip(Pos);
Voc_19 = [594, 664, 778];
V_Tau_778 = [3.943e4, 3.65e4, 1.476e4, 1.919e4, 2.508e4, 2.275e4, 6.316e4, 5.099e4]; %TPV decay Tau Dataset1 Voc=-778 for all positions
V_Tau_664 = [1.825e4, 1.596e4, 1.096e4, 1.386e4, 1.482e4, 1.19e4, 3.451e4, 1.697e4];
V_Tau_594 = [8557, 7999, 5781, 6917, 7002, 7516, 1.289e4, 1.012e4];

B1_19 = flip(V_Tau_778);
B2_19 = flip(V_Tau_664);
B3_19 = flip(V_Tau_594);

Voc = [594, 664, 778];
PosZ_beta = [1.012e4, 1.697e4, 5.099e4];
PosY_beta = [1.289e4, 3.451e4, 6.316e4];
PosA_beta = [7516, 1.19e4, 2.275e4];
PosB_beta = [7002,1.482e4, 2.508e4];
PosC_beta = [6917, 1.386e4, 1.919e4];
PosD_beta = [5781, 1.096e4, 1.476e4];
PosE_beta = [7999, 1.596e4, 3.65e4];
PosF_beta = [8557, 1.825e4, 3.943e4];

pos_voc_arr0 = [Voc; PosZ_beta; PosY_beta; PosA_beta; PosB_beta; PosC_beta; PosD_beta; PosE_beta; PosF_beta];

% DUT5 Amplitude (V) Oct 19 Data Amplitudes obtained from matlab algorithm
Mamp778 = [-0.0016, -5.5087e-4, -9.5525e-5, -3.7669e-5, -1.6465e-4, -2.0916e-4, 1.5562e-4, 4.2348e-4];
Mamp664 = [-0.0211, -0.004, -4.8037e-4, -7.0651e-4, -9.7333e-4, -8.5211e-4, 1.535e-4, 0.0014];
Mamp594 = [-0.0561, -0.0169, -0.0015, -0.0014, -7.2901e-4, -4.1264e-4, 2.9552e-4, 9.9912e-4];
% AMplitudes gotten from oscilloscope P-P measurements pos Y to Pos F (mV)
amp508 = [.674, .267, -.643, -1.751, -2.396, -3.558, -42.22, -83.66];
amp547 = [1.05, 0.5095, -.289, -1.172, -1.8205, -2.4005, -15.5, -49.75];
amp594 = [1.195, 0.770, 0.0215, -0.1265, -1.408, -1.64525, -17.903, -44.78];
amp631 = [1.633, 0.792, 0.825, -.1895, -.9257, -1.0793, -7.9645, -20.797];
amp675 = [1.1663, 0.3167, -0.642, -0.729, -0.8615, -0.936, -4.326, -19.22];
amp780 = [0.649, -0.363, -0.364, -0.218, -0.252, -0.308, -0.643, -1.798];

amp = [amp547; amp594; amp631; amp675; amp778];
figure;
plot(Pos(1:6), amp(4,1:6))
grid on


% Added Nov 5 Data from oct19 never processed
% averaged data Beta
Voc1 = [547, 594, 631, 675]; % \pm 25mV

Y = [6608, 8787, 9386, 1.033e4];
Z = [1.21e4, 9880, 1.026e4, 2.241e4];
```

```
A = [2172, 8654, 6913, 1.515e4];
B = [4491, 4701, 7259, 8833];
C = [5870, 5736, 8864, 9330];
D = [5882, 6108, 7941, 1.028e4 ];
E = [6719, 8390, 1.026e4, 1.259e4];
F = [7504, 8882, 1.186e4, 1.21e4];

pos_voc_arr1 = [Voc1; Y; Z; A; B; C; D; E; F];

% Raw data Beta
YY = [7591, 9983, 8964, 1.0275e4];
ZZ = [1.356e4, 9696, 1.115e4, 2.241e4];
AA = [2412, 1.309e4, 7215, 1.812e4];
BB = [5384, 5478, 6586, 1.026e4];
CC = [6063, 6523, 8046, 1.035e4];
DD = [6245, 6999, 7890, 9939];
EE = [6748, 8544, 1.045e4, 1.236e4];
FF = [7851, 8989, 1.242e4, 1.205e4];

pos_voc_arr2 = [Voc1; YY; ZZ; AA; BB; CC; DD; EE; FF];

% Average of the two fitted waveform estimation, bc they come from the same
% dataset
pos_voc_arr = (pos_voc_arr2 + pos_voc_arr1)/2;

% Combine the two 594 mV data to increase confidence
pos_voc_arr(:,2) = (pos_voc_arr0(:,1)+pos_voc_arr2(:,2)+pos_voc_arr1(:,2))/3;

%Standard Deviation of TPV Decay values matrix, rows are Voc, columns are position on device
Std = [630, 846, 298, 1274; 6891, 3387, 629, 883; 170, 3136, 213, 8309; 539, 549, 476, 1009; 200, 556, 568, 721; 296, 886, 361, 241, ; 70, 671, 134, 162; 686, 77, 396, 661];

%%% Complete Dataset
% voc = [547, 594, 631, 675, 594, 664, 778]; %Avg 594s and 675 with 664 = 670
voc = [547, 594, 631, 670, 778];
voc = voc - 70;
%TPV Amplitudes

ya = [0.0011, 0.0011, 0.0015, 0.0012, 4.2348e-4];
za = [2.502e-4, 8.34e-4, 9.145e-4, 5.77e-4, 1.5562e-4];
aa = [6.57e-4, 2.542e-4, 6.92e-4, 4.59e-4, 2.0916e-4];
ba = [0.001, 4.5147e-4, 5.017e-4, 3.282e-4, 1.6465e-4];
ca = [0.0017, 8.42e-4, 7.24e-4, 6.516e-4, 3.7669e-5];
da = [0.0024, 0.0018, 0.0012, 0.0011, 9.5525e-5];
ea = [0.0151, .02, 0.011, 0.0041, 5.5087e-4];
fa = [0.0487, 0.0356, 0.0209, 0.0179, 0.0016];

amp_arr = [ya; za; aa; ba; ca; da; ea; fa];
```

5.2.4 TPC Processing 2

```
Vb = [-2, -1, 0, 1, 2]; %,
Pos = [1.5, 4.5, 7.5, 10.5, 12.5, 15, 17, 19];

Vb_N11 = [-2.35, -1.65, -0.65, 0.35, 0.65, 1.36, 1.65]; %Nov11 data for biased tpc

% Nov 9 Charge collected Current transients integration with applied bias
% voltages
% In Coulombs
Q_f5 = [7.09012436592673e-14, 2.38247641419197e-13, 3.87285006936762e-12, 4.18370226878003e-12, 4.31761690197806e-12];
Q_e5 = [8.52682760124075e-17, 1.49909095511300e-13, 2.28522822337375e-12, 2.42633952600261e-12, 2.50441240147478e-12]; %Shifting up by lowest value for log plots
Q_d5 = [-1.97367377659809e-14, 6.01828305083454e-17, 2.76153186576975e-13, 3.98490568737158e-13, 3.62323895035030e-13];
Q_c5 = [-4.32812778930578e-14, 3.68394690304632e-14, 1.53156432426839e-13, 1.56363926165765e-13, 2.91049750047360e-13];
Q_b5 = [-9.14195036453533e-15, 5.72255427922543e-14, 1.10406196202374e-13, 2.39242322377146e-13, 2.71828190764680e-13];
Q_a5 = [-7.59926400113526e-14, 2.86939177531207e-14, 1.73326138258157e-13, 1.12167381570271e-13, 1.11501895242592e-13];
Q_c5 = [-3.54133710054614e-13, -7.77479443286489e-14, 1.36160001324667e-13, 3.81928744041241e-14, 6.31690239536228e-14];
Q_y5 = [-4.36118507120980e-13, -1.15925086347463e-13, 9.42591142907076e-14, 4.21699739403255e-14, 3.99565188032512e-14];

Q_pos_arr = [Vb; Q_y5; Q_z5; Q_a5; Q_b5; Q_c5; Q_d5; Q_e5; Q_f5]; %trying to disclude olda data

% Nov 11 Bias voltage tpc Vb_N11
qy50 = [-5.36302072652174e-13, -3.33947150717391e-13, 2.11338425000000e-15, 2.54525851869565e-13, 2.29074167608696e-13, 1.46209929717391e-13, 4.67503692391304e-14]; % CAUTION of last 2 elements, check image
qz50 = [-4.63584521695652e-13, -3.76619772000000e-13, -2.39911913043478e-16, 2.65749894673913e-13, -1.35151238152174e-14, -6.52520938478261e-14, -1.95457511510870e-13];% CAUTION of last 2 elements, check image and 3rd last
qa50 = [-1.75451757152174e-13, -1.08862145804348e-13, 1.19277106010870e-13, 2.32561052032609e-13, 1.57759092369565e-13, -1.20405926739130e-13, -2.13165941304348e-15]; % CAUTION of last element, 2nd last needs special attent
qb50 = [-6.13526177173913e-14, -2.77883701739131e-14, 8.78950620217392e-14, 2.10208830521739e-13, 1.90982794586957e-13, 1.82045559076087e-13, 1.45599267326087e-13];
qc50 = [-1.51742288695652e-14, -1.25612499021739e-14, 5.61850919456522e-14, 1.22863339695652e-13, 2.85466062000000e-13, 7.13199861413044e-14, 2.97483547869565e-13];
qd50 = [-2.09476345217391e-14, 1.29146804347826e-14, 8.02590789130436e-14, 1.82807550869565e-13, 3.74232107956522e-13, 2.84793582521739e-13, 3.38880335489131e-13];
qe50 = [2.34895521739131e-14, 1.16670378434783e-13, 1.30362172934783e-13, 3.86591006717391e-13, 5.49475131141304e-13, 1.27741839606522e-12, 1.27546977516304e-12];
qf50 = [5.28991807173912e-14, 1.06058768684783e-13, 2.13235498608696e-13, 6.91308659510870e-13, 9.98444513586957e-13, 2.85307968532609e-12, 4.33446411206522e-12];

q_pos_arr = [Vb_N11; qy50; qz50; qa50; qb50; qc50; qd50; qe50; qf50];

% qy51 = [];
% qz51 = [-4.63214386146133e-13, -3.76040727661153e-13, -1.20956005510409e-14, 2.79610883693190e-13, 6.36644786993950e-14   -4.21545270772722e-14   -1.77042912621774e-13];
% qa51 = [-1.75784929930042e-13, -1.09138424722884e-13, 2.29542129627470e-14, 1.52440847724246e-13, 1.47465171587986e-13, -1.21122040042986e-13, -2.19133380114621e-13];
% qb51 = [-5.48991186357460e-14, -3.31886036004850e-14, 3.39760777837449e-14, 1.52106190218862e-13, 1.88691568975684e-13, 2.02034598494383e-13, 1.51891424135497e-13];
% qc51 = [-2.31841329509436e-14, -1.60985212238086e-14, 3.93585470914978e-14, 1.28747865776192e-13, 2.89833685348047e-13, 7.37087570492977e-14, 3.02666847980452e-13];
% qd51 = [-1.86627167232715e-14, 1.31669445242786e-14, 2.42738555209789e-14, 2.12441024311506e-13, 3.75038226869898e-13, 2.87129014631056e-13, 3.41481855162558e-13];
% qe51 = [2.54706204500506e-14, 5.50022872794023e-14, 6.84063102367971e-14, 3.45852040257773e-13, 4.95948730734218e-13, 1.27694986645145e-12, 1.27845973121765e-12];
% qf51 = [4.13996662545420e-12, 5.39642349791464e-14, 1.12914644237865e-13, 5.72548940006454e-13, 8.37241077140002e-13, 2.84782699833942e-12, 4.13996662545420e-12];
V_bias = sort([Vb_N11, Vb]);
% Q_arr = [V_bias; q_pos_arr(2:9,1)  q_pos_arr(2:9,2) q_pos_arr(2:9,3) q_pos_arr(2:9,4) q_pos_arr(2:9,5) q_pos_arr(2:9,6) q_pos_arr(2:9,7) Q_pos_arr(2:9,1)];
%Q_arr = [V_bias; q_pos_arr(2:9,1x  q_pos_arr(2:9,2) Q_pos_arr(2:9,2) q_pos_arr(2:9,3) Q_pos_arr(2:9,3) q_pos_arr(2:9,4) q_pos_arr(2:9,5) Q_pos_arr(2:9,4) q_pos_arr(2:9,6) q_pos_arr(2:9,7) Q_pos_arr(2:9,5)];

%Nov 9 TPC Data, Transients collected at various Voc, voc9 no bias voltage.
%The Voc is just to equate an illumination, the circuit was not open
voc9 = [540, 590, 640, 690, 770] - 70;
```

```
% Charge collected. Each arr is a certain voc across voc0(1) = posY, voc0(end) = posF
voc0_770 = [2.55695834106334e-13, 3.31157919256226e-13, 2.93036437185943e-13, 1.68152127036052e-13, 2.24975078991407e-13, 2.36111562128871e-13, 6.97192091868912e-13, 1.96538739946977e-12];
voc1_770 = [2.52608720753825e-13, 3.28040899162647e-13, 2.89408431815570e-13, 1.65665016688904e-13, 2.22404257446548e-13, 2.35539992710556e-13, 6.93076941661470e-13, 1.95311230654986e-12];
voc0_690 = [4.17270229713042e-13, 1.16168038913956e-12, 2.04036472234989e-12, 2.87309323915697e-12, 3.86348203546282e-12, 4.79140087527644e-12, 1.69325536547603e-11, 3.38989761826449e-11];
voc1_690 = [4.15055605135778e-13, 1.15605447246564e-12, 2.03325012224259e-12, 2.86045574858744e-12, 3.84955296470523e-12, 4.77316755518077e-12, 1.68701818799444e-11, 3.37798251862507e-11];
voc0_640 = [1.55174069515947e-13, 2.34408172651757e-13, 5.41148108825210e-13, 9.51406177933779e-13, 1.40197744483159e-12, 2.03871200409527e-12, 2.43085587148276e-11, 3.95069567537607e-11];
voc1_640 = [1.51852991201967e-13, 2.34598697384633e-13, 5.38399964274459e-13, 9.47616018545387e-13, 1.39495807691166e-12, 2.03064369712096e-12, 2.42270143237519e-11, 3.93718826229791e-11];
voc0_590 = [1.24097509154924e-13, 1.39807979095911e-13, 2.18598714888277e-13, 5.27498248206636e-13, 9.90375317108117e-13, 1.28188454286570e-12, 1.93587889654500e-11, 4.36754092323702e-11];
voc1_590 = [1.21674531606183e-13, 1.38269401687752e-13, 2.19095145000737e-13, 5.23205848863403e-13, 9.82447458538973e-13, 1.27810267180624e-12, 1.92848795412128e-11, 4.35203485777133e-11];
voc0_540 = [1.45369700607618e-14, 8.68782472247134e-14, 2.71354356955129e-13, 6.77177851078026e-13, 8.53217180778638e-13, 1.68055567248395e-12, 1.45434943175569e-11, 4.24347986722202e-11];
voc1_540 = [1.30236668646747e-14, 8.63836021732679e-14, 2.69743846191619e-13, 6.72179635136382e-13, 8.49585597493843e-13, 1.67447510308103e-12, 1.44903567447710e-11, 4.22866335509690e-11];

q_arr0 = [voc0_540; voc0_590; voc0_640; voc0_690; voc0_770];
q_arr1 = [voc1_540; voc1_590; voc1_640; voc1_690; voc1_770];
%Plot of charge vs position for Vbi Determination
% figure;
% % plot(Q_pos_arr(1,1:2), Q_pos_arr(8,1:2),'-x','LineWidth',2)
% plot(Q_pos_arr(1,:), Q_pos_arr(2,:),'-x','LineWidth',2)
% grid on
% legend('1 $\mu$m','4 $\mu$m','7 $\mu$m','10 $\mu$m','12 $\mu$m','15 $\mu$m','18 $\mu$dm','21 $\mu$m','Interpreter','latex','Location','northwest');%
% % title('DUT5 TPC Charge Collected $\beta$ vs Vb','Interpreter','latex');
% title('DUT5 Linear Fit of Low Bias Voltage Data (Nov 9)','Interpreter','latex');
% xlabel('Vb (V)','Interpreter','latex');
% ylabel('Charge Collected (C)','Interpreter','latex');
% % ylim([-1.5e-13,4.5e-12]);
% xlim([-2.8,-0.6]);

% qf = fittype({'x'});
fq = fit(transpose(q_pos_arr(1:1,3:4)),transpose(q_pos_arr(9:9,3:4)),'linearinterp');
figure;
plot(fq, q_pos_arr(1:1,:), q_pos_arr(9,:), 'x')
% plot(q_pos_arr(1,1:3), q_pos_arr(8,1:3), '-x','LineWidth',2)
grid on
% legend('1 $\mu$m','4 $\mu$m','7 $\mu$m','10 $\mu$m','12 $\mu$m','15 $\mu$m','18 $\mu$dm','21 $\mu$m','Interpreter','latex','Location','northwest');%
% title('DUT5 TPC Charge Collected $\beta$ vs Vb','Interpreter','latex');
legend('18 $\mu$dm','Fit','Interpreter','latex','Location','northwest');%
title('DUT5 Linear Fit of Low Bias Voltage Hecht Plot $x$ = 18 $\mu$dm','Interpreter','latex','FontSize',20);
xlabel('Vb (V)','Interpreter','latex','FontSize',16);
ylabel('Charge Collected (C)','Interpreter','latex','FontSize',16);
ax = gca;
ax.ColorOrder = mycolors;
% set(gca,'Color',[0.9, 0.9, 0.9])
% ylim([-1.3e-13,2.3e-13]);
% xlim([-3,-0.6])
% Plot of charge collected vs position
```

```
fq = fit(transpose(q_pos_arr(1:1,3:4)),transpose(q_pos_arr(9:9,3:4)),'linearinterp');
figure;
plot(fq, q_pos_arr(1:1,:), q_pos_arr(9,:), 'x')
% plot(q_pos_arr(1,1:3), q_pos_arr(8,1:3), '-x','LineWidth',2)
grid on
% legend('1 $\mu$m','4 $\mu$m','7 $\mu$m','10 $\mu$m','12 $\mu$m','15 $\mu$m','18 $\mu$dm','21 $\mu$m','Interpreter','latex','Location','northwest');%
% title('DUT5 TPC Charge Collected $\beta$ vs Vb','Interpreter','latex');
legend('18 $\mu$dm','Fit','Interpreter','latex','Location','northwest');%
title('DUT5 Linear Fit of Low Bias Voltage Hecht Plot $x$ = 18 $\mu$dm','Interpreter','latex');
xlabel('Vb (V)','Interpreter','latex');
ylabel('Charge Collected (C)','Interpreter','latex');
ax = gca;
ax.ColorOrder = mycolors;
set(gca,'Color',[0.9, 0.9, 0.9])
% ylim([-1.3e-13,2.3e-13]);
% xlim([-3,-0.6])
% Plot of charge collected vs position
% plot(Pos, Q_pos_arr(2:9,:), '-x','LineWidth',2)
% grid on
% legend('Vb = -2 V','Vb = -1 V','Vb = 0 V','Vb = 1 V','Vb = 2 V','Interpreter','latex');
% title('DUT5 TPC Charge Collected $\beta$ vs Position','Interpreter','latex');
% xlabel('Position ($\mu$m)','Interpreter','latex');
% ylabel('Charge Collected (C)','Interpreter','latex');

% plot(voc9,q_arr0(:,1))
```

5.2.5 TPV and TPC Processing

```
T = 300; % K
elementay_charge = 1.6*10^-19;
k_B = 1.3792*10^-23; % Boltzmanns Constant
%%%%   TPV DATA from DUT5_Analysis_Nov12 %%%%
Pos = [1.5, 4.5, 7.5, 10.5, 12.5, 15, 17, 19]; %Position in micrometers
pos = [1, 3.25, 5.5, 7.75, 10, 12.25, 14.5, 16.75]; % New estimate Nov13
voc = [547, 594, 631, 670, 778];
voc = voc - 70; %Subtracting the offset voc

voc9 = [540, 590, 640, 690, 770]; % Voc from TPC Data
voc9 = voc9 - 70;
%%% AMPLITUDE DATA %%%

% Amplitudes gotten from oscilloscope P-P measurements (mV), Ordered
amp508 = [.674, .267, -.643, -1.751, -2.396, -3.558, -42.22, -83.66];
amp547 = [1.05, 0.5095, -.289, -1.172, -1.8205, -2.4005, -15.5, -49.75];
amp594 = [1.195, 0.770, 0.0215, -0.1265, -1.408, -1.64525, -17.903, -44.78];
amp631 = [1.633, 0.792, 0.825, -.1895, -.9257, -1.0793, -7.9645, -20.797];
amp675 = [1.1663, 0.3167, -0.642, -0.729, -0.8615, -0.936, -4.326, -19.22];
amp780 = [0.649, -0.363, -0.364, -0.218, -0.252, -0.308, -0.643, -1.798];
amp = [amp547; amp594; amp631; amp675; amp778].*10^-3; % For units in Volts

% MATLAB TPV Amplitudes (V)
ya = [0.0011, 0.0011, 0.0015, 0.0012, 4.2348e-4];
za = [2.502e-4, 8.34e-4, 9.145e-4, 5.77e-4, 1.5562e-4];
aa = [6.57e-4, 2.542e-4, 6.92e-4, 4.59e-4, 2.0916e-4];
ba = [0.001, 4.5147e-4, 5.017e-4, 3.282e-4, 1.6465e-4];
ca = [0.0017, 8.42e-4, 7.24e-4, 6.516e-4, 3.7669e-5];
da = [0.0024, 0.0018, 0.0012, 0.0011, 9.5525e-5];
ea = [0.0151, .02, 0.011, 0.0041, 5.5087e-4];
fa = [0.0487, 0.0356, 0.0209, 0.0179, 0.0016];
amp_arr = [ya; za; aa; ba; ca; da; ea; fa];

%%% TPV DECAY DATA %%%

% y corresonds to 1um, f to 20um, 1um is small area contact, 20um is large
y = [5969, 9630, 9175, 1.253e4, 5.099e4];
z = [1.083e4, 10822, 10705, 2.6443e4, 6.316e4];
a = [3351, 9753.3, 7064, 1.506e4, 2.275e4];
b = [4987.5, 5727, 6922.5, 1.73e4, 2.508e4];
c = [6244, 6392, 8455, 1.118e4, 1.919e4];
d = [5851, 6296, 7915.5, 1.0393e4, 1.476e4];
e = [6654, 8311, 1.0355e4, 1.5637e4, 3.65e4];
f = [7213, 8809, 1.214e4, 1.8133e4, 3.943e4];
barr = [y; z; a; b; c; d; e; f];
%TPV Decay uncertanties
```

```
%TPV Decay uncertanties
std = [1375, 846, 298, 2561, 2827; 6891, 3387, 629, 3887, 1.131e4; 1027, 3136, 213, 5710, 5799; 408, 549, 476, 2068,
    8309; 551, 556, 568, 1549, 2475; 260, 886, 361, 380, 1526; 121, 671, 134, 1089, 7411; 699, 77, 396, 2113, 3315];

% Apparent electron lifetimes matrix
tarr = (1./barr).*((k_B*T)/elementay_charge);
arr = [voc; tarr];

% Apparent electron lifetimes uncertainties
stdt = (std./arr(2:end,:)).*arr(2:end,:);
%%%%%%%%%%%%%%%%%%%%%%%%%%%%


%%%%%% TPC DATA from DUT5_TPC_Analysis_Ot30
Vb = [-2, -1, 0, 1, 2]; %Nov9 TPC bias voltages
Vb_N11 = [-2.35, -1.65, -0.65, 0.35, 0.65, 1.36, 1.65]; %Nov11 TPC bias voltages
V_bias = sort([Vb_N11, Vb]); % combined bias voltages Nov 9 & 11
% (Nov 9 TPC Data) Transients collected at various Voc "voc9" no bias voltage.
% 0 signifies data, 1 signifies averaged data

%The Voc is just to equate an illumination, the circuit was not open
%voc9 = [540, 590, 640, 690, 770];
% Charge collected. Each arr is a certain voc across voc0(1) = posY, voc0(end) = posF
voc0_770 = [2.556958341063e-13, 3.311579192562e-13, 2.930364371859e-13, 1.681521270360e-13, 2.249750789914e-13, 2.361115621288e-13, 6.971920918689e-13, 1.965387399469e-12];
voc1_770 = [2.526087207538e-13, 3.280408991626e-13, 2.894084331855e-13, 1.656650166889e-13, 2.224042574465e-13, 2.355399927105e-13, 6.930769416614e-13, 1.953112306549e-12];
voc0_690 = [4.172702297130e-13, 1.161680389135e-12, 2.040364722349e-12, 2.873093239156e-12, 3.863482035462e-12, 4.791400875276e-12, 1.693255365476e-11, 3.389897618264e-11];
voc1_690 = [4.150556051357e-13, 1.156054472465e-12, 2.033250122242e-12, 2.860455748587e-12, 3.849552964705e-12, 4.773167555180e-12, 1.687018187994e-11, 3.377982518625e-11];
voc0_640 = [1.551746095159e-13, 2.344081726517e-13, 5.411481088252e-13, 9.514061779337e-13, 1.401977444831e-12, 2.038712004095e-12, 2.430855871482e-12, 3.950695675376e-11];
voc1_640 = [1.518529912019e-13, 2.345986973846e-13, 5.383999642745e-13, 9.476160185453e-13, 1.394958076911e-12, 2.030643697120e-12, 2.422701432375e-11, 3.937188262297e-11];
voc0_590 = [1.240975091549e-13, 1.398079790959e-13, 2.185987144888e-13, 5.274982482066e-13, 9.903753171081e-13, 1.281884542865e-12, 1.935878896545e-11, 4.367540923237e-11];
voc1_590 = [1.216745316061e-13, 1.382694016877e-13, 2.190951450007e-13, 5.232058488634e-13, 9.824474585389e-13, 1.278102671806e-12, 1.928487954121e-11, 4.352034857711e-11];
voc0_540 = [1.453697006076e-14, 6.687824722471e-14, 2.713543569551e-13, 6.771778510780e-13, 8.532171807786e-13, 1.680555672483e-12, 1.454349431755e-11, 4.243479867222e-11];
voc1_540 = [1.302366686467e-14, 6.638360217326e-14, 2.697438461916e-13, 6.721796351368e-13, 8.495855974938e-13, 1.674475103081e-12, 1.449035674771e-11, 4.228663355096e-11];
% q_arr0 = [voc0_540; voc0_590; voc0_640; voc0_690; voc0_770];
q_arr1 = [voc1_540; voc1_590; voc1_640; voc1_690; voc1_770];
q_arr0 = [voc0_540; voc0_590; voc0_640; voc0_690; voc0_770].*0.0285; %This is a factor to help with the overestimate of a 100kohm resistor
% it is the ratio of the extrapolated true TPC decay over the 100kohm
% TPCdecay
% Nov 9 Charge collected Current transients integration with applied bias
% voltages
% In Coulombs
Q_f5 = [7.090124365926 73e-14, 2.382476414191976e-13, 3.87285006936762e-12, 4.183702268780 03e-12, 4.317616901978 06e-12];
Q_e5 = [8.526827601240 73e-17, 1.499090955113 00e-13, 2.285228223373 75e-12, 2.426339526002 61e-12, 2.504412401474 78e-12]; %Shifting up by lowest value for log plots
Q_d5 = [-1.973673776598 09e-14, 6.018283050834 54e-17, 2.761531865769 75e-13, 3.984905687371 58e-13, 3.623238930350 30e-13];
Q_c5 = [-4.328127789305 78e-14, 3.683946903046 32e-14, 1.531564324268 39e-13, 1.563639261657 65e-13, 2.910497500473 60e-13];
Q_b5 = [-9.141950364535 33e-15, 5.722554279225 43e-14, 1.104061962023 74e-13, 2.392423223771 46e-13, 2.718281907646 80e-13];
```

```
Q_a5 = [-7.59926400113526e-14, 2.86939177531207e-14, 1.73326138258157e-13, 1.12167381570271e-13, 1.11501895242592e-13];
Q_z5 = [-3.54133710054614e-13, -7.77479443286489e-14, 1.36160901324667e-13, 3.81928744041241e-14, 6.31690239536228e-14];
Q_y5 = [-4.36118507120980e-13, -1.15925086347463e-13, 9.42591142907076e-14, 4.21699739403255e-14, 3.99565188032512e-14];

Q_pos_arr = [Vb; Q_y5; Q_z5; Q_a5; Q_b5; Q_c5; Q_d5; Q_e5; Q_f5]; %trying to disclude olda data

% Nov 11 Bias voltage tpc Vb_N11
qy50 = [-5.36302072652174e-13, -3.33947150717391e-13, 2.11338425000000e-15, 2.54525851869565e-13, 2.29074167608696e-13, 1.46209929717391e-13, 4.67503692391304e-14]; % CA
qz50 = [-4.63584521695652e-13, -3.76619772000000e-13, -2.39911913043478e-16, 2.65749894673913e-13, -1.35151238152174e-14, -6.52520938478261e-14, -1.95457511510870e-13];%
qa50 = [-1.75451757152174e-13, -1.08862145804348e-13, 1.19277106010870e-13, 2.32561052032609e-13, 1.57759092369565e-13, -1.20405926739130e-13, -2.13165941304348e-15]; %
qb50 = [-6.13526177173913e-14, -2.77883701739131e-14, 8.78950620217392e-14, 2.10208830521739e-13, 1.90982794586957e-13, 1.82045359076087e-13, 1.45599267326087e-13];
qc50 = [-1.51742288695652e-14, -1.25612499021739e-14, 5.61850919456522e-14, 1.22863339695652e-13, 2.85466062000000e-13, 7.13199861413044e-14, 2.97483547869565e-13];
qd50 = [-2.09476345217391e-14, 1.29146804347826e-14, 8.02590789130436e-14, 1.82807550869565e-13, 3.74232107956522e-13, 2.84793582521739e-13, 3.38880335489131e-13];
qe50 = [2.34895521739131e-14, 1.16670378434783e-13, 1.30362172934783e-13, 3.86591006717391e-13, 5.49475131141304e-13, 1.27741839606522e-12, 1.27546977516304e-12];
qf50 = [5.28991807173912e-14, 1.06058768684783e-13, 2.13235498608696e-13, 6.91308659510870e-13, 9.98444513586957e-13, 2.85307968532609e-12, 4.33446411206522e-12];

q_pos_arr = [Vb_N11; qy50; qz50; qa50; qb50; qc50; qd50; qe50; qf50];
%%%%%%%%%%%%%%%%%%%%%%%%%%%%%%%%%%%%%
%%%%% COMBINED DATA ANALYSIS %%%%%%%%

d1 = 30*10^-9; % Device thickness from 1um to 15um
d2 = 60*10^-9; % Device thickness from 17 to 20 um
Spotsize = (pi*10^-4)^2;

dq_dv = q_arr0./transpose(amp_arr); % Divide charge extracted by transient voltage peak
% Columns are positions, rows are the summed charges upto that voc

qvoc = cumtrapz(voc9.*1*10^-3,dq_dv,1); % Integrate over dv_dq from voc1 to vocN for N=1 to N

% Charge density at each position (Col) and Voc (row) in SI units
% Divide charges by elementary charge, thickness, and contact
% area->estimated to be contact width times thickness
nvoc = [qvoc(:,1:6)./(elementay_charge*d1*6.67*10^-6), qvoc(:,7:8)./(elementay_charge*d2*13.68*10^-6)];
nvoc = nvoc.*(1*10^-6); % put units in cm^-3
% Need to plot the loglog so take abs(nvoc)
Nvoc = abs(nvoc);

% Log-Log plots of carrier liftimes dependence on carrier density
%%% THIS IS WHAT I'VE BEEN WAITING FOR %%%
mycolors = [1 0.25 0.5; 0.25 1 0.5; 0.5 0.25 1; 1 1 0.25; 1 0.5 1; 0.5 1 1; 1 0.5 0.25; 0.5 .5 0.25];
figure;
loglog(Nvoc,transpose(arr(2:9,:)),'-*','LineWidth',2)
grid on
legend('1 $\mu$m','4 $\mu$m','7 $\mu$m','10 $\mu$m','12 $\mu$m','15 $\mu$m','18 $\mu$m','21 $\mu$m','Interpreter','latex','Location','northeast');%
title('DUT5 Carrier Lifetime Dependence on Charge Density','Interpreter','latex');
xlabel('Charge Density (cm$^{-3}$)','Interpreter','latex');
```

```
xlabel('Charge Density (cm$^{-3}$)','Interpreter','latex');
ylabel('Carrier Lifetimes $\tau_n$ (sec)','Interpreter','latex');
ax = gca;
ax.ColorOrder = mycolors;
% Not sure which one is better -> im going with above because the liftimes
% get slightly shorter at less charge density for some reason.

%%%%%%%%%%%%%% OLD but keeping %%%%%%%%%%%%%%%%%
% Nvoc = nvoc - min(nvoc,[],2);
% figure;
% loglog(Nvoc,transpose(arr(2:9,:)),'-*','LineWidth',2)
% grid on
% legend('1 $\mu$m','4 $\mu$m','7 $\mu$m','10 $\mu$m','12 $\mu$m','15 $\mu$m','18 $\mu$dm','21 $\mu$m','Interpreter','latex','Location','northeast');%
% title('DUT5 Carrier Lifetime Dependence on Charge Density','Interpreter','latex');
% xlabel('Charge Density (cm$^{-3}$)','Interpreter','latex');
% ylabel('Carrier Lifetimes ($\tau_n$)','Interpreter','latex');
% ax = gca;
% set(gca,'Color',[0.9, 0.9, 0.9])
% ax.ColorOrder = mycolors;
%%%%%%%%%%%%%%%%%%%%%%%%%%%%%%%%%%%%%%%%%%%%%%%%%%%%%%%%%%%%%%%

%%%%%%%%%%%%%%%%%%%%%%%%%%%%%%%%%%%%%%
%%%%%%% ELECTRIC FIELD ANALYSIS %%%%%%

%Dataset 1 from Nov 11 (V) element(1) = posY element(8) = PosF
Vbi1_N11 = [-0.65629, -0.6491, -1.1728, -1.409799, -1.4675, -1.9169, -3.065546, -2.853]; %Method of extraction 1 (black)
Vbi2_N11 = [-0.65629, -0.6491, -1.75, -1.409799, -1.4675, -1.45, -1.2, -1.2]; %Method of extraction 2 (red)
OCV_N11 = -0.690; %Offset subtracted
%TPC was performed under illumination bias, subtract OCV from extracted Vbi (OR subtract it from the bias voltage when extracting Vbi)
Vbi1_N11 = Vbi1_N11 - OCV_N11;
Vbi2_N11 = Vbi2_N11 - OCV_N11;

%Dataset 2 from Oct 30
Vbi1_O30 = [-0.448459, -0.6365, -1.274093, -1.86225, -1.4599, -1.00034, -2, -2.424];
Vbi2_O30 = [-0.448459, -0.6365, -1.225, -2.083, -1.33, -1, -1.1, -1.142];
OCV_O30 = -0.673; %The premeasurement Voc was 705, the post measurement Voc was 640 with offset subtracted avg = -.673
Vbi1_O30 = Vbi1_O30 - OCV_O30;
Vbi2_O30 = Vbi2_O30 - OCV_O30;

%Average datasets
Vbi1 = (Vbi1_N11 + Vbi1_O30)./2;
Vbi2 = (Vbi2_N11 + Vbi2_O30)./2;
```

```
% Built in Electric Field estimation
% Need to consider which contact electrons are collected at to consider
% distance, pos 1 and 2 electrons move toward small and 3 to 8 they move
% toward large contact, therefore distance travelled is p(1), p(2),
% 20-[p(3) to p(8)] in um
distance5 = [pos(1:2), 20-pos(3:8)].*10^-6;
E1_D5 = Vbi1./distance5;
E2_D5 = Vbi2./distance5;

%%%%trying shifting up E to be positive inly for log plots%%%%
% E1_D5 = E1_D5 - min(E1_D5);
% E2_D5 = E2_D5 - min(E2_D5);
% figure;
% semilogy(pos,E1_D5,'-*','LineWidth',2)
% figure;
% semilogy(pos,E2_D5,'-*','LineWidth',2)
% semilogx(pos,E1_D5)
% hold on
% semilogx(pos,E2_D5)
%%%%%%%%%%%%%%%%%%%%%%%%%%%%%%%%%%%%%%%%%%%%%%%%%%%%%%%%%%%%%%%%%%%%%%%
figure;
plot(pos(1:8),E1_D5(1:8),'-*','LineWidth',2)
grid on
title('DUT5 Built in Electric Field Strength','Interpreter','latex');
xlabel('Position ($\mu$m)','Interpreter','latex');
ylabel('Electric Field Strength (V/m)','Interpreter','latex');
figure;
plot(pos(1:8),E2_D5(1:8),'-*','LineWidth',2)
grid on
title('DUT5 Built in Electric Field Strength','Interpreter','latex');
xlabel('Position ($\mu$m)','Interpreter','latex');
ylabel('Electric Field Strength (V/m)','Interpreter','latex');

% figure;
% plot(voc9,E2_D5(1:8),'-*','LineWidth',2)
% grid on
% title('DUT5 Built in Electric Field Strength','Interpreter','latex');
% xlabel('Position ($\mu$m)','Interpreter','latex');
% ylabel('Electric Field Strength (V/m)','Interpreter','latex');
```

Bibliography

[1] J. Xu, Y. Peng, S. Qian, and L. Jiang, "Microstructured all-optical switching based on two-dimensional material," *Coatings*, vol. 13, no. 5, 2023.

[2] Ossila, "Molybdenum disulfide (mos2): Theory applications." Retrieved from `https://www.ossila.com/en-ca/pages/molybdenum-disulfide-mos2#:~:text=MoS2%20occurs%20naturally%20as,often%20used%20as%20a%20lubricant`.

[3] A. Abnavi, R. Ahmadi, H. Ghanbari, M. Fawzy, A. Hasani, T. De Silva, A. M. Askar, M. R. Mohammadzadeh, F. Kabir, M. Whitwick, M. Beaudoin, S. K. O'Leary, and M. M. Adachi, "Flexible high-performance photovoltaic devices based on 2d mos2 diodes with geometrically asymmetric contact areas," *Advanced Functional Materials*, vol. 33, no. 7, p. 2210619, 2023.

[4] L. Hao, Y. Liu, Z. Han, Z. Xu, and J. Zhu, "Giant lateral photovoltaic effect in mos2/sio2/si p-i-n junction," *Journal of Alloys and Compounds*, vol. 735, pp. 88–97, 2018.

[5] T. Bronger, *Time-of-Flight Analysis*, ch. 9, pp. 203–229. John Wiley Sons, Ltd, 2011.

[6] C. Zhou, S. Raju, B. Li, M. Chan, Y. Chai, and C. Y. Yang, "Self-driven metal–semiconductor–metal wse2 photodetector with asymmetric contact geometries," *Advanced Functional Materials*, vol. 28, no. 45, p. 1802954, 2018.

[7] T. Chowdhury, E. C. Sadler, and T. J. Kempa, "Progress and prospects in transition-metal dichalcogenide research beyond 2d," *Chemical Reviews*, vol. 120, no. 22, pp. 12563–12591, 2020.

[8] H. J. Conley, B. Wang, J. I. Ziegler, R. F. J. Haglund, S. T. Pantelides, and K. I. Bolotin, "Bandgap engineering of strained monolayer and bilayer mos2," *Nano Letters*, vol. 13, no. 8, pp. 3626–3630, 2013. PMID: 23819588.

[9] W. Chen, E. J. G. Santos, W. Zhu, E. Kaxiras, and Z. Zhang, "Tuning the electronic and chemical properties of monolayer mos2 adsorbed on transition metal substrates," *Nano Letters*, vol. 13, no. 2, pp. 509–514, 2013.

[10] H. J. S. J. H. T. Mak KF, Lee C, "Atomically thin mos: a new direct-gap semiconductor," *Physical review letters*, vol. 105, 2010 Sep 24.

[11] P. Phalswal, P. K. Khanna, H.-G. Rubahn, and Y. K. Mishra, "Nanostructured molybdenum dichalcogenides: a review," *Mater. Adv.*, vol. 3, pp. 5672–5697, 2022.

[12] S. Han, R. Bhatia, and S.-W. Kim, "Synthesis, properties and potential applications of two-dimensional transition metal dichalcogenides," *Nano Convergence*, vol. 2, 12 2015.

[13] S. Yang, S. Tongay, Y. Li, Q. Yue, J.-B. Xia, S.-S. Li, J. Li, and S.-H. Wei, "Layer-dependent electrical and optoelectronic responses of rese2 nanosheet transistors," *Nanoscale*, vol. 6, pp. 7226–7231, 2014.

[14] J. W. Ryan and E. Palomares, "Photo-induced charge carrier recombination kinetics in small molecule organic solar cells and the influence of film nanomorphology," *Advanced Energy Materials*, vol. 7, no. 10, p. 1601509, 2017.

[15] E. Palomares, N. F. Montcada, M. Méndez, J. Jiménez-López, W. Yang, and G. Boschloo, "Chapter 7 - photovoltage/photocurrent transient techniques," in *Characterization Techniques for Perovskite Solar Cell Materials* (M. Pazoki, A. Hagfeldt, and T. Edvinsson, eds.), Micro and Nano Technologies, pp. 161–180, Elsevier, 2020.

[16] A. Zaban, M. Greenshtein, and J. Bisquert, "Determination of the electron lifetime in nanocrystalline dye solar cells by open-circuit voltage decay measurements," *ChemPhysChem*, vol. 4, no. 8, pp. 859–864, 2003.

[17] X. Xue, Y. Nie, B. He, L. Xing, Y. Zhang, and Z. L. Wang, "Surface free-carrier screening effect on the output of a zno nanowire nanogenerator and its potential as a self-powered active gas sensor," *Nanotechnology*, vol. 24, p. 225501, apr 2013.

[18] S. A. Svatek, C. Bueno-Blanco, D.-Y. Lin, J. Kerfoot, C. Macías, M. H. Zehender, I. Tobías, P. García-Linares, T. Taniguchi, K. Watanabe, P. Beton, and E. Antolín, "High open-circuit voltage in transition metal dichalcogenide solar cells," *Nano Energy*, vol. 79, p. 105427, 2021.

[19] R. Dagan, Y. Vaknin, A. Henning, J. Y. Shang, L. J. Lauhon, and Y. Rosenwaks, "Two-dimensional charge carrier distribution in MoS2 monolayer and multilayers," *Applied Physics Letters*, vol. 114, p. 101602, 03 2019.

[20] R. Dagan, Y. Vaknin, A. Henning, J. Shang, L. Lauhon, and Y. Rosenwaks, "Two-dimensional charge carrier distribution in mos 2 monolayer and multilayers," *Applied Physics Letters*, vol. 114, p. 101602, 03 2019.

[21] G.-H. L. Y. D. K. G. A. P. Y. H. C.-H. L. D. A. C. e. a. Cui, Xu, "Multi-Terminal Transport Measurements of MoS2 Using a van Der Waals Heterostructure Device Platform.," *Harvard FAS Articles*, p. 50, 4 2015.

[22] S. Karazhanov, "Impurity photovoltaic effect in indium-doped silicon solar cells," *Journal of Applied Physics*, vol. 89, pp. 4030–4036, 04 2001.

[23] H. Wang, C. Zhang, and F. Rana, "Surface recombination limited lifetimes of photoexcited carriers in few-layer transition metal dichalcogenide mos2," *Nano Letters*, vol. 15, no. 12, pp. 8204–8210, 2015. PMID: 26535607.

[24] N. Kumar, J. He, D. He, Y. Wang, and H. Zhao, "Charge carrier dynamics in bulk MoS2 crystal studied by transient absorption microscopy," *Journal of Applied Physics*, vol. 113, p. 133702, 04 2013.

[25] H. Shi, R. Yan, S. Bertolazzi, J. Brivio, B. Gao, A. Kis, D. Jena, H. G. Xing, and L. Huang, "Exciton dynamics in suspended monolayer and few-layer mos2 2d crystals," *ACS Nano*, vol. 7, no. 2, pp. 1072–1080, 2013. PMID: 23273148.

[26] O. Sandberg, K. Tvingstedt, P. Meredith, and A. Armin, "A theoretical perspective on transient photovoltage and charge extraction techniques," *The Journal of Physical Chemistry C*, vol. 123, 05 2019.